PLANT SCIENCES

A dynamic ubiquitination balance of cell proliferation and endoreduplication regulators determines plant organ size

Ying Chen[1,2], Mattias Vermeersch[1,2], Jelle Van Leene[1,2], Geert De Jaeger[1,2], Yunhai Li[3], Hannes Vanhaeren[1,2,4]*

Ubiquitination plays a crucial role throughout plant growth and development. The E3 ligase DA2 has been reported to activate the peptidase DA1 by ubiquitination, hereby limiting cell proliferation. However, the molecular mechanisms that regulate DA2 remain elusive. Here, we demonstrate that DA2 has a very high turnover and auto-ubiquitinates with K48-linkage polyubiquitin chains, which is counteracted by two deubiquitinating enzymes, UBIQUITIN-SPECIFIC PROTEASE 12 (UBP12) and UBP13. Unexpectedly, we found that auto-ubiquitination of DA2 does not influence its stability but determines its E3 ligase activity. We also demonstrate that impairing the protease activity of DA1 abolishes the growth-reducing effect of DA2. Last, we show that synthetic, constitutively activated DA1-ubiquitin fusion proteins overrule this complex balance of ubiquitination and deubiquitination and strongly restrict growth and promote endoreduplication. Our findings highlight a nonproteolytic function of K48-linked polyubiquitination and reveal a mechanism by which DA2 auto-ubiquitination levels, in concert with UBP12 and UBP13, precisely monitor the activity of DA1 and fine-tune plant organ size.

INTRODUCTION

After the synthesis and folding of proteins, their function and fate can be affected by a broad range of posttranslational modifications (PTMs), which offer a broad array of flexible fine-tuning in the proteomic landscape. Although PTMs can be irreversible, such as cleavage by endo- and exoproteases, resulting in the protein's maturation (*1*, *2*), relocalization (*3*), or degradation (*4*, *5*), most of the PTMs are reversible, which allows a swift and dynamic tweaking of the proteome and greatly avoids the energy-demanding synthesis of new proteins. Among the more than 200 PTMs, ubiquitination plays a fundamental role in various eukaryotic biological processes by modulating protein stability, activity and localization, protein complex assembly, and DNA repair (*6*–*10*).

Ubiquitination is mediated by an enzymatic cascade, including ubiquitin-activating enzymes (E1), ubiquitin-conjugating enzymes (UBC and E2), and ubiquitin ligases (E3) (*11*). First, the 76–amino acid polypeptide ubiquitin is activated by an E1 in an adenosine 5′-triphosphate (ATP)–dependent manner and transferred to an E2. Subsequently, the substrate-determining E3 ligase brings the E2 in proximity of a target protein and facilitates the covalent binding of the ubiquitin molecule on a lysine residue. Monoubiquitinations can be further extended on one of the seven lysine residues of ubiquitin (K6, K11, K27, K29, K33, K48, and K63) or on the N-terminal methionine by additional covalently linked ubiquitin molecules, hereby forming single or branched ubiquitin chains (*12*, *13*). These various types of ubiquitination, such as monoubiquitination, multi-monoubiquitination, and polyubiquitination with different ubiquitin chain linkages, can trigger various effects on the modified proteins. For example, K48- and K11-linked chains are typically associated with proteasomal degradation (*14*, *15*); K63-linked chains are known to regulate proteasome-independent pathways, such as autophagy, signal transduction, and DNA repair (*16*–*18*). Besides homotypic chains, in which the ubiquitin molecules are consistently linked to the same acceptor site of the previous ubiquitin, heterotypic ubiquitin chains have been shown to direct proteolytic as well as nonproteolytic signaling (*19*). E2 enzymes play a crucial role in determining the linkage specificity of the polyubiquitin chain (*19*–*21*). For instance, the human E2s Ube2C/UbcH10 and Ube2S (*15*, *22*) and the *Arabidopsis* homolog UBC22 (*23*) are able to catalyze K11-linked ubiquitination. An in vitro ubiquitination assay showed that AtUBC10 can conjugate both K48 and K63 linkages, while AtUBC35 mostly prefers K63 sites (*24*).

E3 ligases are the most diverse protein group of the ubiquitination cascade. While more than 600 genes are predicted to encode E3 ligases in the human genome and 70 genes in yeast, *Arabidopsis* encodes approximately 1400 (*5*, *25*), indicating the prominent role of the ubiquitination machinery in plant proteostasis. E3 ligases can be subdivided into three groups: the homology to E6-AP C-terminal type, the really interesting new gene (RING)/U-box domain type, and the RING-between-RING (RBR) type (*26*). Most of the E3 ligases contain a RING domain, which is essential for their interaction with the E2~ubiquitin intermediates (*5*) and for their own auto-ubiquitination (*27*). Several studies in humans and *Arabidopsis* have demonstrated that E3 ligases regulate their own stability by auto-ubiquitination (*28*–*30*).

Ubiquitination is a dynamic and reversible modification. Deubiquitination enzymes (DUBs) can process ubiquitin precursors, recycle ubiquitin, or polyubiquitin chains and proofread ubiquitin conjugation (*31*). According to their protein domains and action mechanisms, DUBs can be divided into seven subfamilies: the ubiquitin C-terminal hydrolases (UCHs), the ubiquitin-specific proteases (USPs/UBPs), the ovarian tumor domain–containing proteases (OUTs), the Josephin domain–containing proteases (MJDs), zinc finger with UFM1-specific peptidase domain proteases (ZUFSPs), motif-interacting with

[1]Ghent University, Department of Plant Biotechnology and Bioinformatics, Technologiepark 71, B-9052 Ghent, Belgium. [2]VIB Center for Plant Systems Biology, Technologiepark 71, B-9052 Ghent, Belgium. [3]State Key Laboratory of Plant Cell and Chromosome Engineering, CAS Centre for Excellence in Molecular Plant, Institute of Genetics and Development Biology, Chinese Academy of Sciences, Beijing 100101, China. [4]Department of Biotechnology, Faculty of Bioscience Engineering, Ghent University, Proeftuinstraat 86, 9000 Ghent, Belgium.
*Corresponding author. Email: hannes.vanhaeren@ugent.be

ubiquitin-containing novel DUB family (MINDY), and JAB1/MPN/MOV34 metalloenzymes (JAMMs) (*32*, *33*). In different species, the number of E3 ligases surpasses the variety of DUBs, but this difference is notably pronounced in plants. In humans and yeast, around 100 and 20 DUBs, respectively, are described, whereas only 64 DUBs have been identified so far in *Arabidopsis* (*34*, *35*), indicating that DUBs can target various substrates in different contexts. Studies on the role of DUBs in plants have substantially gained momentum in the past years, highlighting the impact of these enzymes on development (*36*). For example, UBP6 and UBP7 deubiquitinate the transcriptional coactivator NONEXPRESSOR OF PATHOGENESIS RELATED GENES 1, hereby increasing its stability and downstream responses (*37*). UBP14 interacts with ULTRAVIOLET-B INSENSITIVE4, a negative regulator of the anaphase-promoting complex/cyclosome (*38*), and stabilizes CYCLIN-DEPENDENT KINASE B1;1 to restrict endoreduplication (*39*). Plant growth is reduced in *ubp15* mutants, whereas overexpression of *UBP15* increases cell proliferation and leads to larger organs (*40*, *41*). UBP12 and UBP13, which share more than 90% of sequence similarity and work redundantly (*42*), have recently been shown to be involved in several regulatory pathways. UBP12 and UBP13 deubiquitinate and stabilize several key players in development and hormone signaling (*32*). For example, UBP12 and UBP13 promote jasmonate signaling by reducing the degradation of the transcription factor MYC2 (*43*), enhance brassinosteroid signaling by reducing the turnover of BRASSINOSTEROID INSENSITIVE 1 (BRI1) (*44*) and BRI1-EMS-SUPPRESSOR 1 (BES1) (*45*, *46*), and regulate abscisic acid signaling by stabilizing VACUOLAR PROTEIN SORTING 23A (VPS23A) and its E3 ligase XB3 ortholog 5 in *Arabidopsis* (XBAT35.2) (*47*). UBP12 and UBP13 are also crucial for maintaining root meristem development by increasing the stability of ROOT MERISTEM GROWTH FACTOR 1 (RGF1) (*48*) and promote leaf senescence under nitrate starvation by reducing proteolysis of ORE-SARA1 (ORE1) (*49*). Other than stabilizing substrates, UBP12 and UBP13 have been shown to regulate the negative growth regulators DA1, DA1-RELATED 1 (DAR1), and DAR2 (*50*). These proteases are activated upon ubiquitination by the E3 ligases BIG BROTHER (BB) and DA2 (*51*), leading to the cleavage of downstream regulators of cell proliferation and endoreduplication, such as UBP15 and several TEOSINTE BRANCHED 1, CYCLOIDEA AND PCF (TCP) proteins (*40*, *51*, *52*). This process can be counteracted by UBP12 and UBP13, which deubiquitinate and hence limit the activation of these proteases (*50*). As an additional layer of control, DA1 can cleave its activating E3 ligases, BB and DA2 (*51*).

In *Arabidopsis*, *da2-1*, the T-DNA insertion loss-of-function mutant of *DA2*, has been demonstrated to produce larger seeds, flowers, and higher plants (*51*, *53*). In addition, in several crop species, such as rice, wheat, and maize, homologs of DA2 were found to regulate seed size (*54*–*59*). Despite its important role in plant yield, surprisingly little is known about the regulation of this E3 ligase. Here, we present that DA2 has a very high turnover and auto-ubiquitinates with K48-linked polyubiquitin chains, which is the primary proteasome-targeting signal. Unexpectedly, this auto-ubiquitination does not affect the stability of DA2 proteins, but modifies its enzymatic activity toward its substrate DA1, demonstrating a proteasome-independent role for K48 ubiquitin linkage. Furthermore, we found that DA2 interacts with UBP12 and UBP13, which were previously identified to deubiquitinate and inactivate DA1 (*50*). UBP12 and UBP13 were found to counteract the auto-ubiquitination of DA2, hereby fine-tuning its catalytic activity. In addition, we demonstrate that impairing the protease activity of DA1 acts epistatic toward the phenotype of *DA2* overexpression lines, showing that DA2 restricts growth uniquely through DA1. Last, we could overrule this complex in vivo ubiquitination/deubiquitination balance in this growth-regulating pathway by generating a constitutively ubiquitin-activated DA1 that strongly restricts organ growth and promotes endoreduplication. Together, our findings indicate an unexpected role for K48 ubiquitin linkage as a PTM and provide insightful perspectives into the complex regulation of plant organ size.

RESULTS

DA2 regulates the transition from cell proliferation to differentiation and endoreduplication

Previous research in *Arabidopsis* has shown that DA2 negatively regulates seed size by limiting cell proliferation in the maternal integuments (*53*). To further investigate the role of DA2 in leaf growth, we phenotyped the loss-of-function mutant *da2-1* and plants overexpressing *DA2* from the 35*S* cauliflower mosaic virus promoter (*35S::DA2*). At 21 days after stratification (DAS), *da2-1* plants produced a larger rosette than Col-0, while *35S::DA2* plants were reduced in growth (Fig. 1A). Leaf area measurements indicated that *da2-1* mutants had larger leaves, whereas the leaves of *35S::DA2* plants were smaller (Fig. 1, A and B), which is consistent with previous observations (*53*). The final size of leaves is determined by two cellular processes, cell proliferation and cell expansion (*60*). To further explore the cellular mechanisms that underlie the observed leaf phenotypes, we performed a cellular analysis on the abaxial pavement cells of the third true leaf at 21 DAS. We confirmed that isolated leaves of *da2-1* plants were significantly larger, whereas those of *35S::DA2* were significantly decreased in size (Fig. 1C). Furthermore, we observed a significant increase in pavement cell number in *da2-1* leaves, whereas *35S::DA2* leaves contained fewer cells (Fig. 1D). The pavement cell area remained unchanged in both genotypes (Fig. 1E).

Next, we analyzed the ploidy levels of leaf cells in Col-0, *da2-1*, and *35S::DA2*. For this purpose, we harvested a time course of the first leaf pair of these lines from 9 DAS to 21 DAS, which covers all major developmental time points (*60*). At 9 DAS, the nuclei of all three lines exhibited a 2C or 4C content, demonstrating that most cells were still in the mitotic cell cycle (Fig. 1F). However, *35S::DA2* displayed a smaller proportion of nuclei with a 2C content and a larger proportion with 4C cells than Col-0 (Fig. 1F). From 12 DAS onward, 8C and 16C nuclei started to appear in all three lines, indicating the onset of endoreduplication. At 12 DAS, the *35S::DA2* line contained a smaller proportion of 4C cells and a larger proportion of 8C cells than Col-0, and from 15 DAS onward, it exhibited a larger proportion of 16C cells and a smaller proportion of 4C cells than Col-0. In contrast, the *da2-1* mutant had slightly more 4C and fewer 8C nuclei compared to Col-0 (Fig. 1F). In general, significantly higher ploidy levels could be observed in *35S::DA2* leaves, whereas slightly lower ploidy levels were found in *da2-1* leaves at an early developmental stage. In conclusion, these results show that DA2 negatively regulates the mitotic cell cycle and promotes endoreduplication in leaves.

The E3 ligase DA2 auto-ubiquitinates on multiple lysines surrounding its RING domain with K48-linkage ubiquitin chains

To uncover the linkage type of ubiquitination and thus the potential biological effect of DA2 auto-ubiquitination, we expressed DA2 and

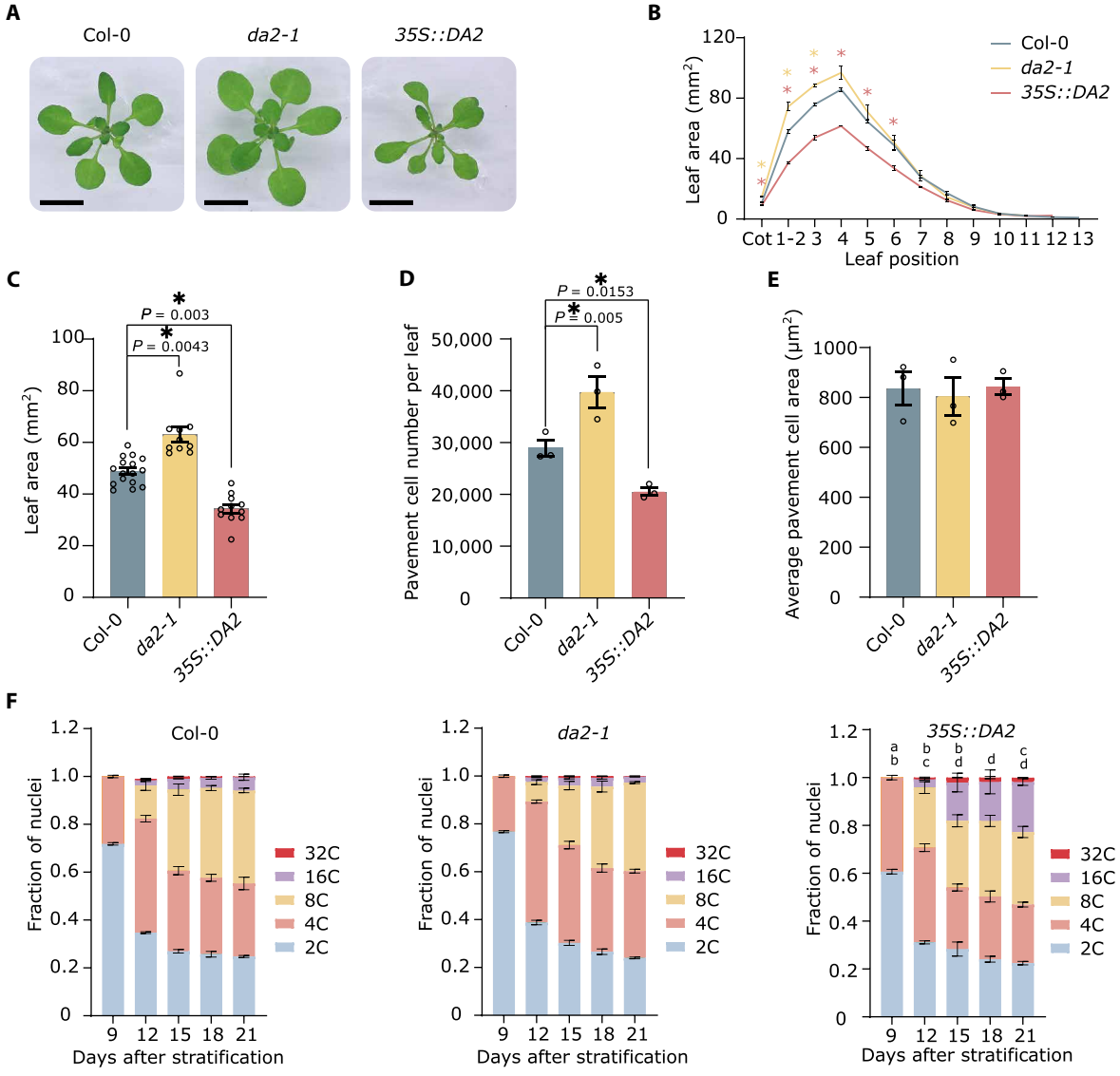

Fig. 1. DA2 negatively regulates leaf growth by limiting cell proliferation. (**A**) Twenty-one-day-old plants of Col-0, *da2-1*, and *35S::DA2*. Scale bars, 1 cm. (**B**) Leaf area measurements of Col-0, *da2-1*, and *35S::DA2* at 21 DAS. Cot, cotyledons. $N = 3$ biological replicates with 10 plants per replicate. Asterisks in yellow or in orange indicate a significant difference of *da2-1* or *35S::DA2* with Col-0, respectively, as determined by analysis of variance (ANOVA) with Dunnett test, $P < 0.05$. (**C**) Average leaf 3 area of Col-0, *da2-1*, and *35S::DA2* at 21 DAS. $N = 3$ biological replicates with >8 plants per replicate. (**D**) Average leaf 3 pavement cell number of Col-0, *da2-1*, and *35S::DA2* at 21 DAS. $N = 3$ biological replicates with three representative leaves per replicate. (**E**) Average pavement cell area of Col-0, *da2-1*, and *35S::DA2* leaves at 21 DAS. $N = 3$ biological replicates with three representative leaves per replicate. (**F**) Ploidy distribution of nuclear DNA in Col-0, *da2-1*, and *35S::DA2* leaf cells. $N = 3$ biological replicates with >3 representative leaves per replicate. In (C) to (E), asterisks indicate a significant difference of *da2-1* or *35S::DA2* with Col-0 as determined by ANOVA with Dunnett test, $P < 0.05$. In (F), a, b, c, and d indicate a significant difference in 2C, 4C, 8C, or 16C fractions, respectively, of *35S::DA2* with Col-0 as determined by ANOVA with Tukey test, $P < 0.05$. Bars represent the SEM.

$DA2^{C59S}$ in *Escherichia coli* as fusion proteins with an N-terminal hexahistidine-maltose–binding protein (HIS-MBP) tag. The $DA2^{C59S}$ protein was mutagenized in its RING domain, leading to an abolished E3 ligase activity (*53*). In the presence of E1, E2 (human UbcH5b), and hemagglutinin (HA)–ubiquitin, we could observe polyubiquitination of HIS-MBP-DA2, but not of HIS-MBP-$DA2^{C59S}$ (Fig. 2A), indicating that auto-ubiquitination of DA2 was abolished in HIS-MBP-$DA2^{C59S}$. We analyzed these ubiquitinated proteins with mass spectrometry (MS) to identify the ubiquitinated lysine residues of DA2, based on the GlyGly mark that remains after trypsin digest. We found that multiple lysines at the N terminus of DA2, within and surrounding the RING domain, were ubiquitinated (Fig. 2B and table S1).

Next, we performed an in vitro auto-ubiquitination assay with C-terminally 6xHIS-tagged DA2 (DA2-HIS) and used chain-specific antibodies against K48- or K63-linked polyubiquitins, which are the most common linkage types (*13*), to elucidate the polyubiquitin chain type. We found that DA2 auto-ubiquitinates with a preference of K48- to K63-linked polyubiquitin chains (Fig. 2C). Furthermore, we could confirm K48-linked polyubiquitin chains of in vitro auto-ubiquitinated

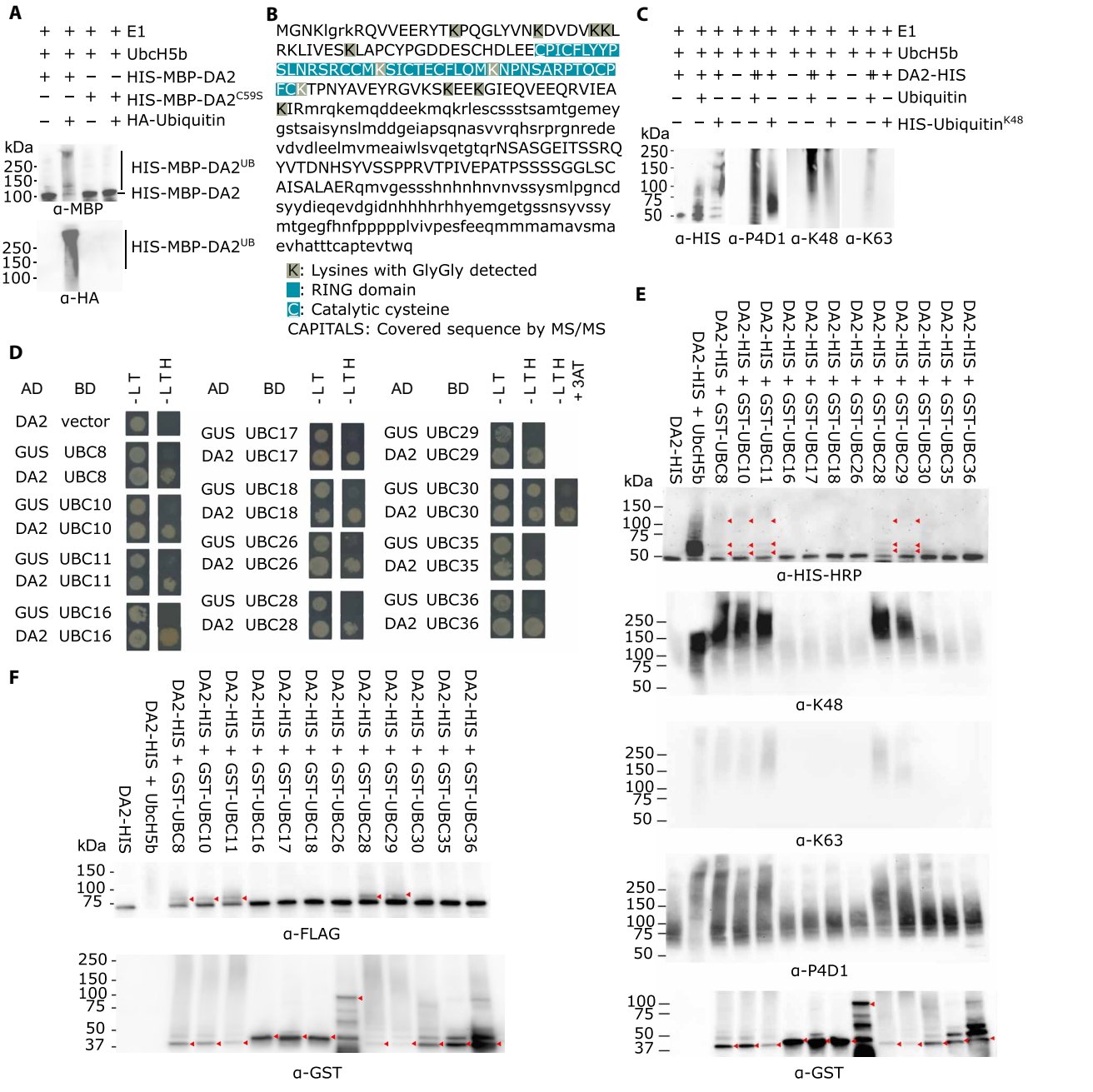

Fig. 2. DA2 interacts with several *Arabidopsis* subgroup VI E2 enzymes to confer ubiquitination. (**A**) In vitro auto-ubiquitination assay of HIS-MBP-DA2 and HIS-MBP-DA2^{C59S}. (**B**) Schematic representation of ubiquitinated lysines (K) on DA2 identified by LC-MS; the sequence covered by MS/MS is indicated in capital letters. (**C**) Ubiquitin chain linkage of DA2-HIS auto-ubiquitination. HIS-Ubiquitin^{K48} indicates ubiquitin in which all lysine residues except K48 are mutated. (**D**) Interaction between *Arabidopsis* endogenous E2 enzymes and DA2 in a yeast two-hybrid screen. AD, activating domain; BD, binding domain; −LT, leucine/threonine dropout; −LTH, leucine/threonine/histidine dropout; 3AT, 3-aminotriazole, 10 mM. (**E**) In vitro auto-ubiquitination assay of DA2 by different *Arabidopsis* E2 enzymes. In the α-HIS-HRP blot, red arrowheads indicate ubiquitinated DA2-HIS, and in the α-GST blot the GST-tagged E2s. α-P4D1 was used to detect ubiquitin. (**F**) DA2 ubiquitinates DA1 with *Arabidopsis* endogenous E2s in vitro. In the α-FLAG blot, red arrowheads indicate ubiquitinated HIS-FLAG-DA1^{H418A,H422A}, and in the α-GST blot the GST-tagged E2s.

DA2-HIS by using HIS-ubiquitin^{K48}, in which all lysines but K48 are mutated and thus allow for the formation of only K48-linked ubiquitin chains (Fig. 2C). Because E2 enzymes contribute to the linkage type on ubiquitinated substrates (*21*), we performed a yeast two-hybrid screen to identify the physical interaction between DA2 and endogenous *Arabidopsis* E2 enzymes. The results showed that DA2 could interact with 12 of the 35 tested E2s, including UBC8, UBC10, UBC11, UBC16, UBC17, UBC18, UBC26, UBC28, UBC29, UBC30, UBC35, and UBC36 (Fig. 2D and fig. S1). Subsequently, we generated recombinant glutathione *S*-transferase (GST)–tagged proteins of these E2 enzymes to perform in vitro auto-ubiquitination assays with DA2. We found that UBC8, UBC10, UBC11, UBC28, and

UBC29, which are from the VI subfamily (*61*), mediate auto-ubiquitination of DA2 with K48-linked polyubiquitin chains (Fig. 2E). Given that the peptidase DA1 can be ubiquitinated by DA2, we then investigated whether the auto-ubiquitination of DA2 and the ubiquitination of DA1 by DA2 are mediated by the same E2 enzyme. To prevent the cleavage of DA2 by ubiquitin-activated DA1, the peptidase-deficient mutant of DA1 (HIS-FLAG-DA1^{H418A,H422A}) was used (*51*). This in vitro ubiquitination assay showed that the ubiquitination of DA1 can only be mediated by those five E2s that mediate auto-ubiquitination of DA2 (Fig. 2F). To conclude, we found that DA2 is auto-ubiquitinated with K48-linked polyubiquitin chains and that five *Arabidopsis* endogenous UBCs, i.e., UBC8, UBC10, UBC11, UBC28, and UBC29, mediate both the polyubiquitination of DA2 and the multiple monoubiquitinations of DA1 by DA2.

Auto-ubiquitination of DA2 does not influence its stability, but its E3 ligase activity

Because K48 polyubiquitin chains typically result in proteasomal degradation, we performed a ratiometric protein stability assay with free green fluorescent protein (GFP), GFP-DA2, and GFP-DA2^{C59S}, coexpressed with free mCherry as a control, in *Nicotiana benthamiana* leaves. Although these constructs were controlled by a strong constitutive promoter, we consistently found very low levels of GFP-DA2, indicating a strong turnover of the protein (Fig. 3A). Unexpectedly, we could find no significant difference between the relative GFP/mCherry intensity of DA2 and DA2^{C59S} (Fig. 3, A and B), which indicates that the auto-ubiquitination of DA2 does not influence its stability. To confirm these results, we used a tandem fluorescent protein timer, consisting of a rapid folding superfolder green fluorescent protein (sfGFP) connected to an mCherry, which has a much slower maturation time (*62*), as a reporter for DA2 turnover rates. The constructs of sfGFP-mCherry-DA2, sfGFP-mCherry-DA2^{C59S}, and the free sfGFP-mCherry control were transformed in *Arabidopsis* cell suspension cultures. Similar to our previous results, the ratio of mCherry/sfGFP in sfGFP-mCherry-DA2 and sfGFP-mCherry-DA2^{C59S} was equal and much lower than that of the free sfGFP-mCherry control (Fig. 3C). Next, we checked the ubiquitination status of sfGFP-mCherry-DA2 and sfGFP-mCherry-DA2^{C59S} in *Arabidopsis* protoplasts. After purification of DA2 from the total protein extract, we found that DA2 and DA2^{C59S} can be ubiquitinated in vivo and that, after a 6-hour treatment with the proteasome inhibitor bortezomib (BTZ), ubiquitinated DA2 fusion proteins strongly accumulated (Fig. 3D). An additional detection with specific anti-K48 antibodies confirmed that DA2 and DA2^{C59S} are modified with K48-linked polyubiquitin chains in vivo (Fig. 3D). Subsequently, we normalized the ubiquitinated fraction of the BTZ-treated sfGFP-mCherry-DA2 and sfGFP-mCherry-DA2^{C59S} samples to the abundance of their respective unmodified bands (α-GFP). Here, we could observe a difference of approximately 15 to 20% in ubiquitination intensity between DA2 and DA2^{C59S}, which can be indicative for the auto-ubiquitination activity of DA2 in vivo (Fig. 3D and fig. S3A). Last, we examined the DA2 and DA2^{C59S} protein levels and expression patterns in *Arabidopsis* seedlings by generating translational β-glucuronidase (GUS) reporter fusion lines under the control of the endogenous *DA2* promoter. We performed a histochemical GUS activity assay on *pDA2::DA2-GUS* plants, but we could not detect any signal (Fig. 3E). Similarly, we did not detect any GUS activity in seedlings expressing *pDA2::DA2^{C59S}-GUS* (Fig. 3E), although we could detect the expression of both constructs at the transcript level (Fig. 3F). Therefore, we treated the seedlings for 24 hours with BTZ, after which we could detect similar intensities and patterns of GUS activity in young leaves of *pDA2::DA2-GUS* and *pDA2::DA2^{C59S}-GUS* seedlings (Fig. 3E). These data consistently show that DA2 protein levels are tightly regulated by the proteasome but that its auto-ubiquitination activity does not contribute to its turnover.

Besides regulating protein stability, auto-ubiquitination has been reported to influence E3 ligase activity (*63*). To examine whether auto-ubiquitination of DA2 may affect its ability to ubiquitinate DA1, we followed the ubiquitination levels of DA1 over time, after adding equal amounts of ubiquitin and peptidase-deficient HIS-FLAG–tagged DA1^{H418A,H422A} to DA2 proteins that were either in vitro auto-ubiquitinated for 4 hours (DA2^{UB}) or un-ubiquitinated DA2. When using un-ubiquitinated DA2, we could observe an increase in the amount of ubiquitinated DA1^{H418A,H422A} proteins, indicated by a steady increase in their molecular mass (Fig. 3G, right). When DA2 was already auto-ubiquitinated, much faster rates of DA1 ubiquitination were observed after 15 and 30 min (Fig. 3G, left). However, at 45 and 60 min, coinciding the auto-ubiquitination of DA2, DA1 was more efficiently ubiquitinated in the reaction that initially contained un-ubiquitinated DA2 (Fig. 3G, right).

Next, we explored whether the ubiquitin chain type is crucial for this change in DA2 activity. For this, we performed the same experiment using lysine-deficient (Lys^0) ubiquitin, which prevents the formation of K48-linked polyubiquitin chains on DA2. Unexpectedly, even after 4 hours, we could only observe a small fraction of ubiquitinated DA1 for both monoubiquitinated and un-ubiquitinated DA2 (Fig. 3H), suggesting that monoubiquitinated DA2 is far less catalytically active than K48-polyubiquitinated DA2. To conclude, these results show that auto-ubiquitination of DA2 affects its E3 ligase activity and that K48-linked polyubiquitination chains are crucial for its catalytic efficiency.

UBP12 and UBP13 interact with DA2 and counteract its auto-ubiquitination

To further explore the molecular network around DA2, we performed an affinity purification coupled to an MS (AP-MS) experiment on GS^{Rhino}-DA2 fusion proteins, expressed in *Arabidopsis* cell suspension cultures. Label-free quantification and a comparison against a large control AP-MS dataset of unrelated bait proteins identified a significant enrichment ($P < 0.01$) of several proteasome subunits, which is in line with the high turnover of DA2 (table S2). In addition, we found a strong enrichment of UBP12 and UBP13 (Fig. 4A). To validate the interaction between DA2 and these UBPs, we performed additional coimmunoprecipitation (Co-IP) experiments. We co-expressed mCherry-DA2 with GFP-UBP12, GFP-UBP13, or free GFP (negative control) from the same vector in *Arabidopsis* cell suspension cultures. Western blot analysis after purification with GFP-trap beads showed that mCherry-DA2 could be copurified with either GFP-UBP12 or GFP-UBP13 but not with free GFP (Fig. 4B). Next, we measured the transcript levels of *DA2*, *UBP12*, and *UBP13* during development from leaf primordium initiation to maturity, showing that *UBP12* and *UBP13* are coexpressed with *DA2* during leaf development (fig. S2A). Additional transient expression of GFP-UBP12 or GFP-UBP13 in *N. benthamiana* leaves demonstrated that these proteins colocalize with mCherry-DA2 or DA2-mCherry in the cytoplasm and in the nucleus (fig. S2B). To determine whether UBP12 and UBP13 can interact directly with DA2, we performed in vitro

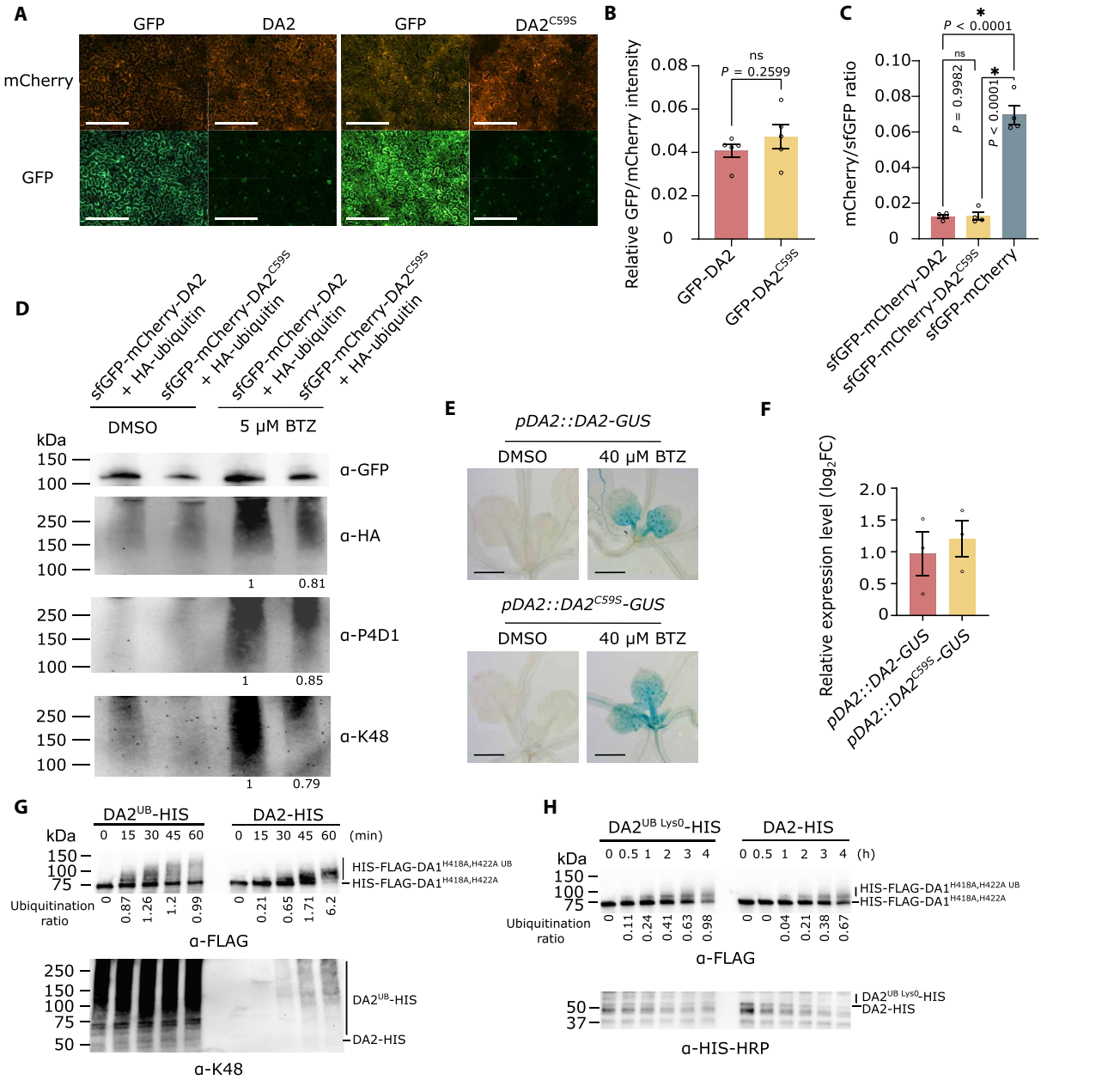

Fig. 3. Auto-ubiquitination of DA2 does not regulate its rapid turnover but modulates its E3 ligase activity. (**A**) Ratiometric fluorescence intensity of free GFP, GFP-DA2, GFP-DA2^{C59S}, and the coexpressed free mCherry as a control in transiently transformed *N. benthamiana* epidermal cells. Scale bars, 200 μm. (**B**) Barplot of the mean GFP/mCherry intensity ratio in the transiently transformed *N. benthamiana* epidermal cells from (A). Bars represent the SEM; $N = 5$ biological replicates. ns, not significant (Student's *t* test). (**C**) Barplot of relative mCherry/sfGFP intensity in *sfGFP-mCherry-DA2*, *sfGFP-mCherry-DA2^{C59S}*, and the free *sfGFP-mCherry* transformed cells. Bars represent the SEM; $N = 4$ biological replicates. $^{**}P < 0.01$ based on ANOVA with Tukey test. (**D**) In vivo ubiquitination status of sfGFP-mCherry-DA2 and sfGFP-mCherry-DA2^{C59S} proteins in *Arabidopsis* protoplasts with or without BTZ treatment. Below lane 3 and 4, relative ubiquitination intensities are shown. (**E**) Histochemical staining of *da2-1* seedlings expressing *pDA2::DA2-GUS* or *pDA2::DA2^{C59S}-GUS* with or without BTZ treatment at 10 DAS. Scale bars, 1 mm. (**F**) Relative transcript expression level of *DA2* in *pDA2::DA2-GUS* and *pDA2::DA2^{C59S}-GUS* at 10 DAS. $N = 3$ biological replicates. (**G**) In vitro ubiquitination assay of HIS-FLAG-DA1^{H418A,H422A} by already polyubiquitinated DA2-HIS (DA2^{UB}-HIS) and unmodified DA2-HIS at time point 0. (**H**) In vitro ubiquitination assay of HIS-FLAG-DA1^{H418A,422A} by multiply-monoubiquitinated DA2-HIS (DA2^{UBLys0}-HIS) and unmodified DA2-HIS at time point 0. In (G) and (H), the amount of ubiquitinated DA1 is calculated as the intensity ratio of ubiquitinated HIS-FLAG-DA1^{H418A,422A}/the intensity of full-length HIS-FLAG-DA1^{H418A,422A}.

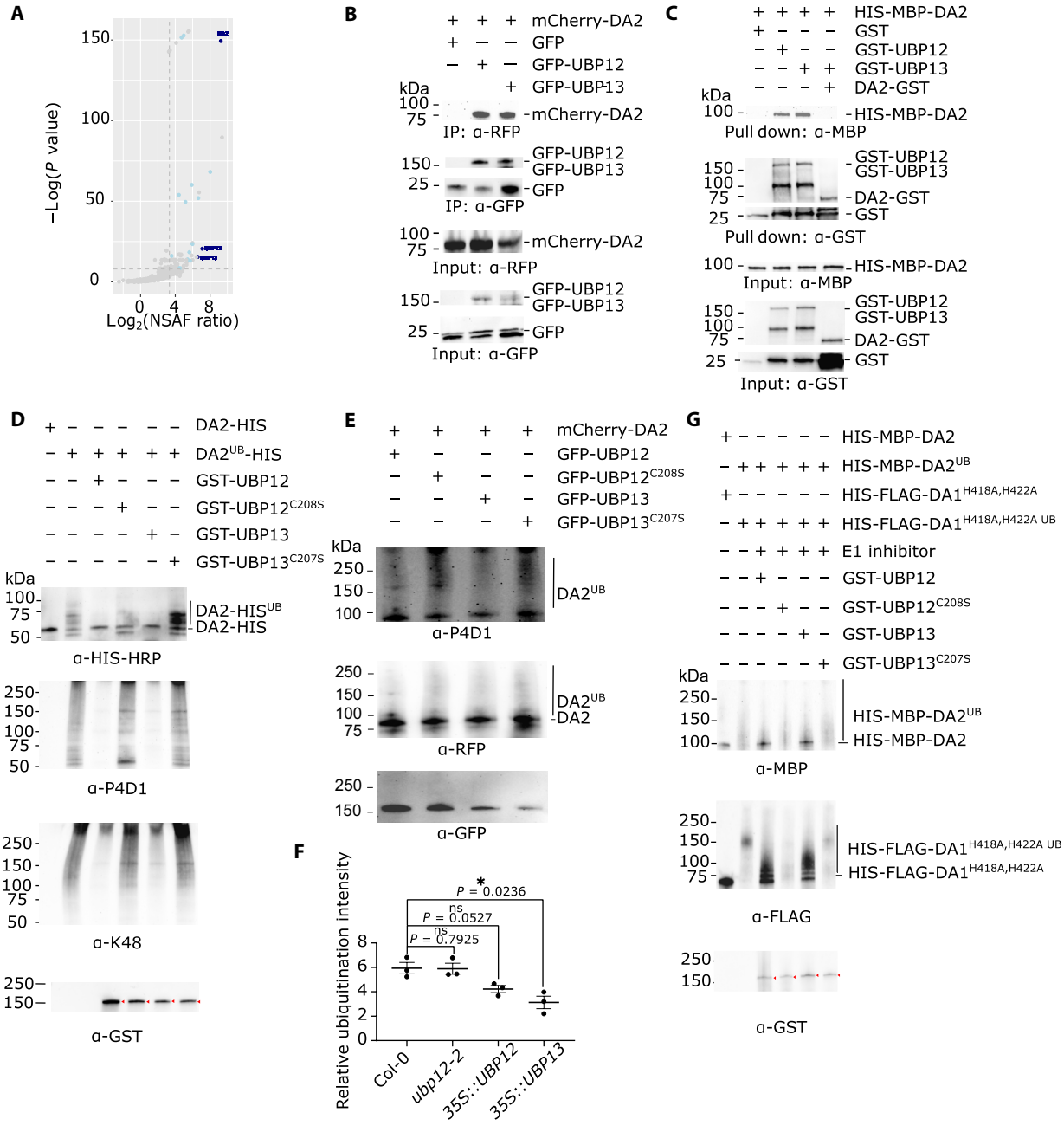

Fig. 4. UBP12 and UBP13 interact with DA2 and counteract its auto-ubiquitination. (**A**) Enrichment of UBP12 and UBP13 compared to the control (large AP-MS dataset with unrelated baits) after AP-MS in *Arabidopsis* cells expressing *35S::GS*^{Rhino}*-DA2*. (**B**) In vivo IP of mCherry-DA2 with free GFP, GFP-UBP12, or GFP-UBP13 in *Arabidopsis* cells. Free GFP was used as a negative control. (**C**) In vitro pull-down of HIS-MBP-DA2 with free GST, GST-UBP12, GST-UBP13, or DA2-GST. Free GST was used as a negative control. (**D**) In vitro deubiquitination assay of auto-ubiquitinated DA2-HIS by GST-UBP12, GST-UBP12^{C208S}, GST-UBP13, or GST-UBP13^{C207S}. (**E**) In vivo deubiquitination assay of mCherry-DA2 by GFP-UBP12, GFP-UBP12^{C208S}, GFP-UBP13, or GFP-UBP13^{C207S} in *Arabidopsis* protoplasts. (**F**) Relative ubiquitination intensity of HIS-MBP-DA2 proteins incubated with cell-free extracts of Col-0, *ubp12-2*, *35S::UBP12*, and *35S::UBP13*. $N = 3$ biological replicates. *$P < 0.05$ based on Student's t test. (**G**) In vitro deubiquitination assay of auto-ubiquitinated HIS-MBP-DA2 and ubiquitinated HIS-FLAG-DA1^{H418A,H422A} by GST-UBP12, GST-UBP12^{C208S}, GST-UBP13, or GST-UBP13^{C207S}. In (D) and (G), red arrowheads in the α-GST blot indicate the full-length GST-tagged UBP proteins.

pull-down assays using recombinant GST-tagged UBP12, UBP13, and DA2 proteins as baits, with free GST as a negative control. These results showed that GST-UBP12 and GST-UBP13, but not the free GST or DA2-GST, pulled down HIS-MBP-DA2 (Fig. 4C), which demonstrates that UBP12 and UBP13 can directly interact with unubiquitinated DA2 and that DA2 does not form homodimers.

UBP12 and UBP13 are DUBs that have been shown to remove ubiquitin from various proteins (*32*). Therefore, UBP12 and UBP13 might counteract the auto-ubiquitination of DA2. To test this hypothesis, we performed an in vitro ubiquitination assay to generate ubiquitinated DA2, followed by a deubiquitination step with UBP12 or UBP13 and their respective catalytic mutants, UBP12^{C208S} and UBP13^{C207S} (*64*).

We could observe that ubiquitinated DA2-HIS was strongly deubiquitinated by GST-UBP12 and GST-UBP13, but not by their respective catalytic mutants (Fig. 4D). Next, we carried out an additional in vitro deubiquitination assay of DA2-HIS with GST-UBP3, GST-UBP15, and GST-UBP24, which are members from different UBP subfamilies (*65*). We found that neither GST-UBP3, GST-UBP15, nor GST-UBP24 had a deubiquitinating activity toward DA2 (fig. S2C), demonstrating the specificity of UBP12 and UBP13.

To demonstrate the ubiquitination and deubiquitination of DA2 in vivo, we cotransfected *Arabidopsis* protoplasts with *35S::mCherry-DA2* and *35S::GFP-UBP12*, *35S::GFP-UBP12*^{C208S}, *35S::GFP-UBP13*, or *35S::GFP-UBP13*^{C207S}, which were treated with BTZ for 6 hours before harvest. After purification of DA2, we observed a strong polyubiquitination on DA2 in the presence of GFP-UBP12^{C208S} and GFP-UBP13^{C207S}, which was reduced in the presence of catalytically active GFP-UBP12 and GFP-UBP13 proteins (Fig. 4E). To further confirm these observations, we evaluated the effect of different in vivo expression levels of *UBP12* and *UBP13* on the ubiquitination status of DA2. To realize this, we incubated recombinant HIS-MBP-DA2 proteins with equal amounts of cell-free protein extracts of Col-0, *ubp12-2*, *35S::UBP12*, and *35S::UBP13* seedlings, supplemented with the proteasomal inhibitor MG132. The *ubp12-2* mutant has reduced transcript levels of both *UBP12* and *UBP13*, as high transcription levels of the 3′ primer region of *UBP12* causes silencing of both *UBP12* and *UBP13* (*64*). After 2 hours, we could observe ubiquitinated HIS-MBP-DA2, shown as an increase of molecular weight, in all four reactions (fig. S3B). The relative intensity of ubiquitinated HIS-MBP-DA2 was similar in the presence of Col-0 and *ubp12-2* extracts (Fig. 4F and fig. S3B). However, in the presence of *35S::UBP12* and *35S::UBP13* extracts, which contain higher levels of UBP12 or UBP13 proteins, respectively, this intensity was lower (Fig. 4F and fig. S3B).

Our previous work showed that UBP12 and UBP13 can deubiquitinate DA1 (*50*), a ubiquitination substrate of DA2. To investigate whether UBP12 and UBP13 have a deubiquitinating preference toward DA1 or DA2, we performed an in vitro deubiquitination assay with HIS-FLAG-DA1^{H418A,H422A} and HIS-MBP-DA2. Equal amounts of HIS-MBP-DA2 and HIS-FLAG-DA1^{H418A,H422A} were incubated with E1, human UbcH5b, ubiquitin, and ATP for 4 hours. Then, MLN7243, an E1 inhibitor, was added to terminate the ubiquitination reaction and GST-UBP12, GST-UBP12^{C208S}, GST-UBP13, or GST-UBP13^{C207S} was added to the reaction mix. After 4 hours, we noticed that the ubiquitin-modified HIS-MBP-DA2 and HIS-FLAG-DA1^{H418A,H422A} were both deubiquitinated by GST-UBP12 and GST-UBP13, but not by GST-UBP12^{C208S} or GST-UBP13^{C207S} (Fig. 4G), indicating that UBP12 and UBP13 deubiquitinate both DA1 and DA2 with no obvious preference.

A synthetic constitutively activated DA1 can overrule the complex ubiquitination balance and restrict growth

The activity of DA1 is regulated by a strict balance between ubiquitination and deubiquitination, which renders in vivo studies of DA1 very complicated. To overrule this complex regulatory network, we aimed to generate a constitutively activated DA1 protein form. Previous research showed that mutating the consistently ubiquitinated lysines of DA1 results in the ubiquitination of alternative lysine residues, still leading to its activation (*51*). This observation shows a certain degree of flexibility toward the position of ubiquitin on DA1, suggesting that the presence of ubiquitin molecules in the proximity of DA1 might be sufficient to switch on its protease activity. To explore this, we generated DA1-ubiquitin fusion constructs, ranging from one to four ubiquitin molecules (DA1-UBI$_{1-4}$) at the C terminus of DA1 (Fig. 5A). Keeping in mind that UBP12 and UBP13 can deubiquitinate DA1, we mutated the double glycine motif at the C terminus of the ubiquitin molecules to valines (UBI^{G75V,G76V}) to prevent endogenous cleavage by deubiquitination enzymes (Fig. 5A). We transformed these constructs in *Arabidopsis* and selected single-locus homozygous lines that overexpressed these protein fusions (fig. S4A). Unexpectedly, we found that most transgenic lines were strongly reduced in growth (fig. S4B). Because a single ubiquitin molecule fused to DA1 (DA1-UBI$_1$) appeared to be sufficient to trigger a strong phenotype, we focused our next experiments on this construct.

Then, we tested whether DA1-UBI$_1$ proteins were constitutively activated. For this purpose, we produced recombinant HIS-FLAG-DA1-UBI$_1$, HIS-FLAG-DA1^{H418A,H422A}-UBI$_1$, and MBP-UBP15-GST and MBP-TCP22-GST proteins as substrates. As a positive and negative control, we used DA2-ubiquinated HIS-FLAG-DA1 and HIS-FLAG-DA1^{H418A,H422A}, respectively. An in vitro cleavage assay showed that HIS-FLAG-DA1 ubiquitinated by DA2 can strongly cleave MBP-UBP15-GST (Fig. 5B) and MBP-TCP22-GST (Fig. 5C), whereas the catalytic mutant shows no cleavage activity (Fig. 5, B and C). We also observed cleaved protein fragments at the same molecular weight in the HIS-FLAG-DA1-UBI$_1$ samples, but not with HIS-FLAG-DA1^{H418A,H422A}-UBI$_1$ (Fig. 5, B and C), demonstrating that a C-terminal fusion of ubiquitin can activate the peptidase activity of DA1.

To gain more insights into the effects of DA1-UBI$_1$ on growth, we phenotypically characterized two independent transgenic lines, *35S::DA1-UBI$_1$ #1* and *35S::DA1-UBI$_1$ #2*, in more detail. Whereas the *da1-1* mutant, which encodes a mutated DA1^{R358K} protein that has been demonstrated to be strongly reduced in its peptidase activity (*51*), produced larger leaves (Fig. 5D), the rosettes and leaf areas of both *35S::DA1-UBI$_1$* lines were reduced (Fig. 5, D and E). In addition, we phenotypically analyzed three independent *35S::DA1* and *35S::GFP-DA1* transgenic lines that showed an equal or higher *DA1* expression level as both *35S::DA1-UBI$_1$* lines (fig. S5A). These results showed that untagged *DA1* overexpression lines were not different in size compared to Col-0 control plants (fig. S5, B to D). In contrast, all *35S::GFP-DA1* overexpression plants were reduced in growth (fig. S5, E to G), albeit not as marked as the *35S::DA1-UBI$_1$* lines.

Next, a cellular analysis on *35S::DA1-UBI$_1$* leaves revealed that the reduction in leaf area was caused by a strong reduction in pavement cell number, combined with a slight reduction in average pavement cell area (Fig. 5, F and G). We further measured the nuclear DNA content in leaves throughout development and found that the ploidy levels were strongly increased in both *35S::DA1-UBI$_1$* lines compared to Col-0 (Fig. 5H). In our previous study (*66*), we measured the ploidy levels of *35S::GFP-DA1* leaves, but no differences in ploidy levels were observed. To unravel the growth-reducing effect of GFP-DA1, we produced recombinant HIS-GFP-DA1 proteins and performed a cleavage assay as described before. Unexpectedly, the HIS-GFP-DA1 proteins also showed cleavage activity toward UBP15 and TCP22 (fig. S6, A and B). Furthermore, we generated a double-tagged HIS-GFP-DA1-UBI$_1$ recombinant protein and performed a similar cleavage assay, but no constitutive cleavage activity could be observed with this fusion protein (fig. S6, A and B). Together, by generating DA1-UBI protein fusions, we could generate constitutive catalytically active DA1 proteoforms that can overrule the complex underlying ubiquitination/deubiquitination mechanisms that strictly regulate the levels of activated DA1.

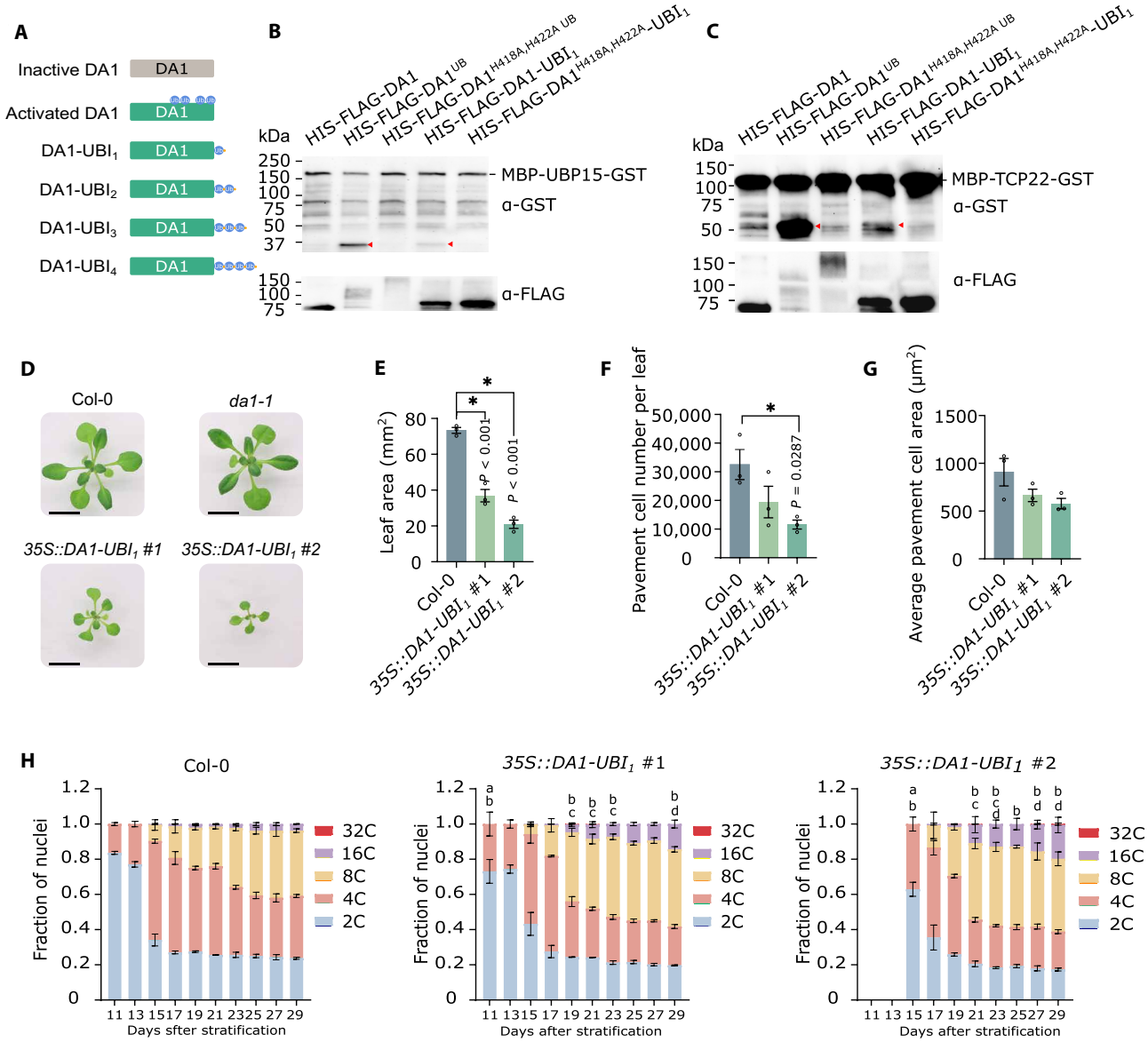

Fig. 5. Synthetic DA1-ubiquitin fusion proteins are constitutively activated and restrict growth. (**A**) Schematic representation of the DA1-ubiquitin fusion proteins. (**B**) In vitro cleavage of MBP-UBP15-GST by HIS-MBP-DA2–mediated ubiquitinated HIS-FLAG-DA1 or HIS-FLAG-DA1^{H418A,H422A} and HIS-FLAG-DA1-UBI$_1$ or HIS-FLAG-DA1^{H418A,H422A}-UBI$_1$ in the absence of HIS-MBP-DA2. (**C**) In vitro cleavage of MBP-TCP22-GST by HIS-MBP-DA2–mediated ubiquitinated HIS-FLAG-DA1 or HIS-FLAG-DA1^{H418A,H422A} and HIS-FLAG-DA1-UBI$_1$ or HIS-FLAG-DA1^{H418A,H422A}-UBI$_1$ in the absence of HIS-MBP-DA2. In (B) and (C), red arrowheads in α-GST blots indicate cleavage products. (**D**) Twenty-one-day-old plants of Col-0, *da1-1*, *35S::DA1-UBI$_1$ #1*, and *35S::DA1-UBI$_1$ #2*. Scale bars, 1 cm. (**E**) Average leaf 3 area of Col-0, *35S::DA1-UBI$_1$ #1*, and *35S::DA1-UBI$_1$ #2* at 21 DAS. $N = 3$ biological repeats with >9 plants per repeat. (**F**) Average leaf 3 pavement cell number of Col-0, *35S::DA1-UBI$_1$ #1*, and *35S::DA1-UBI$_1$ #2* at 21 DAS. $N = 3$ biological repeats with three representative leaves per repeat. (**G**) Average leaf 3 pavement cell area of Col-0, *35S::DA1-UBI$_1$ #1*, and *35S::DA1-UBI$_1$ #2* at 21 DAS. $N = 3$ biological replicates with three representative leaves per replicate. (**H**) Ploidy distribution of nuclear DNA in Col-0, *35S::DA1-UBI$_1$ #1*, and *35S::DA1-UBI$_1$ #2* leaf cells. $N = 3$ biological repeats with three representative leaves per repeat. In (E) and (F), asterisks indicate a significant difference of *35S::DA1-UBI$_1$ #1* or *35S::DA1-UBI$_1$ #2* with Col-0 as determined by ANOVA with Dunnett test, $P < 0.05$. In (H), the letters a, b, c, and d indicate a significant difference in 2C, 4C, 8C, and 16C, respectively, of *35S::DA1-UBI$_1$ #1* or *35S::DA1-UBI$_1$ #2* to Col-0 as determined by ANOVA (Dunnett test, $P < 0.05$). Bars represent the SEM.

The catalytically impairing *da1-1* mutation acts epistatically to *35S::DA2* to determine leaf size, cell proliferation, and endoreduplication

Because E3 ligases can have multiple substrates, it is reasonable to assume that DA2 can also modify other potential growth regulators by ubiquitination, besides DA1. If the growth-reducing effect of DA2 would partially go through other pathways than DA1, blocking the activity of DA1 would not completely restore the reduced growth phenotype of *35S::DA2* plants (Fig. 1). For this purpose, we transformed Col-0 and *da1-1* plants with *35S::DA2* and selected single-locus homozygous lines that displayed similar expression levels (fig. S7A). We also included the previously published *35S::DA2* line (*35S::DA2*) (*53*) in our experiments as a positive control. We could observe a consistent reduced rosette area of the independent *35S::DA2*

overexpression lines (*35S::DA2*/Col-0 #9 and #14) (Fig. 6A). One line that expressed very high levels of *DA2* led to stunted growth (fig. S7, A and B). As described before, the *da1-1* plants produced significantly larger leaves (Fig. 6, A and B). Unexpectedly, the phenotype of *35S::DA2* was completely abolished in the *da1-1* background (Fig. 6, A and B), although the transcripts levels of *DA2* were similar to those in Col-0 (fig. S7A). An additional cellular analysis showed a strong decrease in pavement cell number in all *35S::DA2* lines, whereas the leaves of *da1-1* and both *35S::DA2*/*da1-1* lines contained equally more cells than all *35S::DA2* lines and the Col-0 control (Fig. 6C). Neither *35S::DA2*/*da1-1* nor *35S::DA2*/Col-0 plants showed significant changes in average pavement cell area (Fig. 6D), but the increase of nuclear DNA content in the cells of *35S::DA2* plants was suppressed in the *35S::DA2*/*da1-1* lines (Fig. 6E). These results indicate that DA2 restricts leaf growth and endoreduplication by regulating the catalytic activity of DA1. Together, we demonstrated that DA2 needs functional DA1 proteins to repress growth and increase endoreduplication.

DISCUSSION

DA2 regulates organ size through the peptidase DA1

The E3 ligase DA2 plays a crucial role in regulating seed size in a broad variety of plant species (*51*, *53*–*59*). In this work, we identified several underlying biochemical mechanisms that regulate the activity of DA2 and further elucidate its growth-regulating effect through the peptidase DA1 in *Arabidopsis* leaves. Transcriptional reporters (*53*), quantitative reverse transcription polymerase chain reaction (qRT-PCR) data during leaf development (fig. S2A), and endogenous *DA2*-promoter–driven translational GUS reporters demonstrated that DA2 is under very tight proteasomal control in leaf regions where cells are actively dividing (Fig. 3E). We found that DA2 negatively regulates leaf growth by limiting cell proliferation. The loss-of-function mutant of *DA2*, *da2-1*, formed larger leaves with increased pavement cells, while high ectopic expression of *DA2* led to the formation of smaller leaves with fewer pavement cells and markedly enhanced ploidy levels (Fig. 1).

Considering the importance of ubiquitination in the posttranslational regulation of proteins, E3 ligases often have various substrates. For instance, the *Arabidopsis* E3 ligase CONSTITUTIVE PHOTOMORPHOGENIC 1 (COP1), together with SUPPRESSOR OF PHYA-105 (SPA), targets various substrates, including ELONGATED HYPOCOTYL 5, LONG HYPOCOTYL IN FAR-RED, CONSTANS, and photoreceptors PHYTOCHROME (PHY) A, PHYB, CRYPTOCHROME (CRY) 1, and CRY2 in light signaling (*67*). COP1/SPA also targets ABA INSENSITIVE 1, *bzr1–1D* Suppressor 1, MYC2, and GIBBERELLIC ACID INSENSITIVE, hereby regulating phytohormone signaling (*68*). Similarly, several targets of the homolog of *DA2* in rice, *OsGW2*, have been identified to regulate rice grain size, such as *WIDE GRAIN 1* and *EXPANSIN-LIKE 1* (*57*, *58*). However, our genetic analysis showed that the smaller leaf size, the reduction in cell proliferation, and the increase in endoreduplication levels in *35S::DA2* are completely abolished in the *da1-1* background (Fig. 6). The *da1-1* mutant encodes a mutated $DA1^{R358K}$ protein, which has been demonstrated to be strongly reduced in its peptidase activity (*51*). Mutant *da1-1* plants produce larger leaves that contain more cells (*66*, *69*, *70*), which is phenocopied by *da1ko_dar1-1* double mutants in leaves, but not by the single mutants (*69*). Therefore, this mutation exerts a dominant-negative action toward DA1 and its related proteins (*69*). Because we showed that the *da1-1* phenotype was completely epistatic to that of *35S::DA2* plants in the double transgenic lines, the growth-regulating effect of DA2 on cell proliferation and endoreduplication in leaves requires fully functional DA1 proteins.

K48-linkage auto-ubiquitination regulates the enzymatic activity of DA2

Besides the ability of RING-type E3 ligases to ubiquitinate substrates, auto-ubiquitination is also a general trait of these proteins. Here, we found that DA2 auto-ubiquitinates several lysine residues at its N-terminal part, within and surrounding its RING domain (Fig. 2B), resulting in K48-linked polyubiquitin chains (Fig. 2C). Previous research showed that E2s play a key role in determining the ubiquitination chain type and that ubiquitin chain building is achieved by priming and chain elongation, which can require different E2 enzymes (*20*, *21*). For example, the VI subgroup members can add the first ubiquitin to substrates and perform chain elongation. In contrast, chain-building E2s can only add ubiquitin to substrates, which have been primed, indicating that chain-building E2s can determine the chain type (*21*). UBC8 is a versatile enzyme that can mediate the formation of K11- (*21*), K48-, and K63-linked ubiquitin chains or other even branched linkage types (*71*), while UBC35 and UBC36 mediate primarily K63-linked chains (*72*). Among the 35 AtUBCs that we screened, 12 could associate with DA2 (Fig. 2D). However, only five UBCs (UBC8, UBC10, UBC11, UBC28, and UBC29) belonging to VI subfamily could facilitate K48-linked auto-ubiquitination of DA2 and DA2-mediated ubiquitination of DA1 (Fig. 2, E and F). It is possible that without priming, the interacting chain-building E2s (UBC16, UBC17, UBC18, UBC30, UBC35, and UBC36; Fig. 2D) cannot ubiquitinate DA1 or DA2 in our in vitro screen (Fig. 2, E and F), but they might still play a role in the regulation of DA2 in combination with other E2 enzymes in vivo. The VI subfamily of E2 enzymes shows various expression patterns in vivo (*73*). For example, *UBC8* and *UBC10* are highly expressed in all organs, but most predominantly in leaves, flowers, or roots. On the other hand, *UBC11* shows the highest expression in petals, *UBC28* displays significant higher expression levels in rosette leaves, while *UBC29* is very lowly expressed in rosette leaves (*73*). It is likely that these and the other E2 enzymes interact with DA2 in a cell type–or tissue-specific manner, potentially resulting in additional ubiquitin chain types.

Next, we investigated the molecular consequences of DA2 auto-ubiquitination. Auto-ubiquitination has been found to influence the turnover of E3 ligases (*74*). For example, the E3 ligases AtRING1 and BB were previously shown to be partially stabilized by mutating their RING domain (*30*, *75*) and COP1 could be destabilized by promoting its auto-ubiquitination (*76*). Here, we found that the DA2 protein is very unstable in vivo (Fig. 3, A to E) but can be stabilized by the proteasome inhibitor BTZ (Fig. 3, D and E). In addition, DA2 auto-ubiquitination generates K48-linked ubiquitin chains (Fig. 2C) and several proteasome subunits were identified as interacting proteins (table S2), strongly suggesting that the auto-ubiquitination of DA2 leads to proteasomal degradation. Unexpectedly, abolishing the enzymatic activity and hence auto-ubiquitination of DA2 by mutating its RING domain did not lead to its stabilization in different in vivo contexts (Fig. 3, A to E). Because RING-type E3s can also be ubiquitinated by other E3s and subsequently degraded by the 26*S* proteasome (*74*, *77*), it is likely that the strong

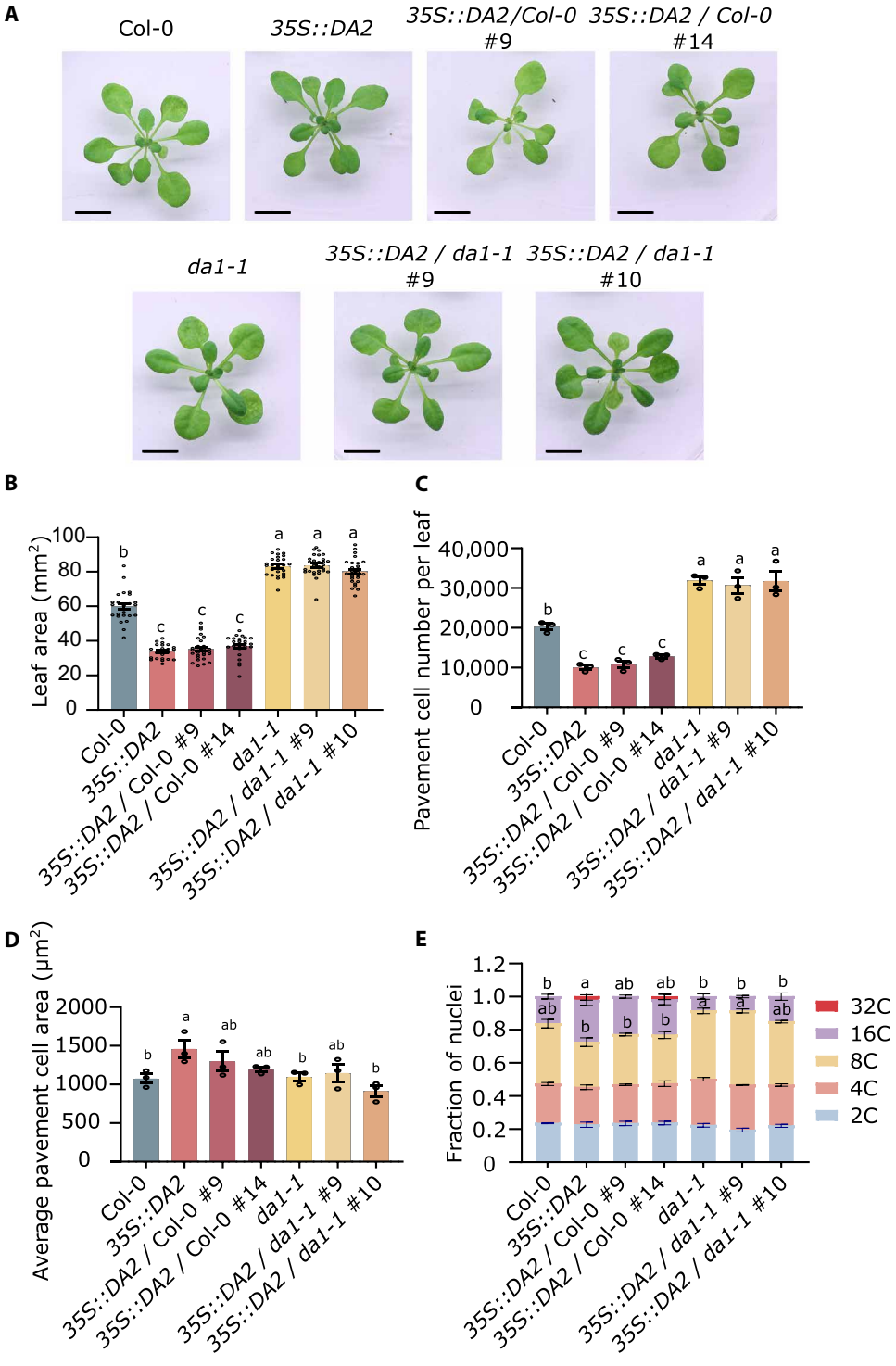

Fig. 6. *da1-1* acts epistatic to *35S::DA2* to determine leaf size, cell proliferation, and endoreduplication. (**A**) Twenty-one-day-old plants of Col-0, *35S::DA2*, two additional independent *DA2* overexpression lines in the Col-0 background (*35S::DA2*/Col-0 #9 and #14), *da1-1*, and *DA2* overexpression lines in the *da1-1* background (*35S::DA2*/*da1-1* #9 and #10). Scale bars, 1 cm. (**B**) Average leaf area of the first leaf pair at 21 DAS. $N = 3$ biological repeats with >9 plants per repeat. (**C**) Average pavement cell number of the first leaf pair at 21 DAS. $N = 3$ biological replicates with three representative leaves per replicate. (**D**) Average pavement cell area of the first leaf pair at 21 DAS. $N = 3$ biological replicates with three representative leaves per replicate. (**E**) Ploidy distribution of nuclear DNA of leaf cells at 21 DAS. $N = 3$ biological replicates with three representative leaves per replicate. In (B) to (D), different letters above the bars indicate significantly different groups as determined by ANOVA followed by Tukey's multiple comparison test, $P < 0.05$. In (E), different letters above the bars indicate significantly different groups in 8C or 16C as determined by ANOVA followed by Tukey's multiple comparison test, $P < 0.05$. Bars represent the SEM.

turnover of DA2 is tightly controlled by other unknown E3 ligases that mark DA2 for proteasomal degradation.

Apart from regulating protein stability, auto-ubiquitination can influence the activity of E3 ligases. Previous studies in mammalian cells have shown that auto-ubiquitination enhances the E3 ligase activity by facilitating the assembly with E2~ubiquitin (*63*, *78*, *79*). However, in *Drosophila melanogaster*, the ligase activity of INHIBITORS OF APOPTOSIS PROTEIN 1 (DIAP1), which inactivates pro-apoptotic regulators, was found to be attenuated by auto-ubiquitination with polymerized ubiquitin chains (*80*). A possible explanation is that polyubiquitin chains in DIAP1 interrupt the interaction between DIAP1 and its substrate, because monoubiquitin modifications did not influence its E3 ligase activity (*80*). Even if K48-type polyubiquitin chains commonly target a protein for 26*S* proteasomal degradation, few proteasome-independent functions of K48 polyubiquitin chains have previously been described. For example, short K48-linked polyubiquitination represses the activity of the budding yeast transcription factor Met4p, but does not lead to its destabilization (*81*, *82*). Here, we observed that auto-ubiquitination of DA2 regulates its activity without altering its stability. Auto-ubiquitination of DA2 with Lys^0 ubiquitin, which prevents further chain building, compromises its activity to multiply monoubiquitinate DA1 (Fig. 3H). On the other hand, K48-linked polyubiquitination of DA2 enhances its activity compared to un-ubiquitinated DA2 (Fig. 3G). We could observe a faster ubiquitination rate of DA1 in the first time points when 4-hour auto-ubiquitinated DA2 was used, compared to un-ubiquitinated DA2 (Fig. 3G).We could observe a sudden increase in ubiquitination rate in samples where DA2 was auto-ubiquitinated for 1 hour (Fig. 3G). These observations suggest a dosage-dependent effect of the auto-ubiquitination status of DA2 on its activity (Fig. 7A). A potential reason can be that very long ubiquitin chains on DA2 might eventually interfere with the interaction between DA2 and DA1 or the E2 enzyme. Similar regulatory mechanisms were observed for the ubiquitination of H2A by RING1B in mammalian cells. To monoubiquitinate H2A, RING1B requires self-ubiquitination, consisting of K6, K27, K48, mixed, and multiple branched chains. However, when Lys^0 ubiquitin was used and no chains could be formed, no monoubiquitination of H2A could be detected (*83*, *84*).

UBP12 and UBP13 regulate growth by limiting the activity of DA2 and DA1

Ubiquitination is a very diverse and reversible PTM, which is fine-tuned by different deubiquitination enzymes (*32*). Over the past years, it has become clear that DUBs play an important role in plant growth and development (*33*). Our affinity purification experiment, using DA2 as a bait, revealed a strong interaction with UBP12 and UBP13,

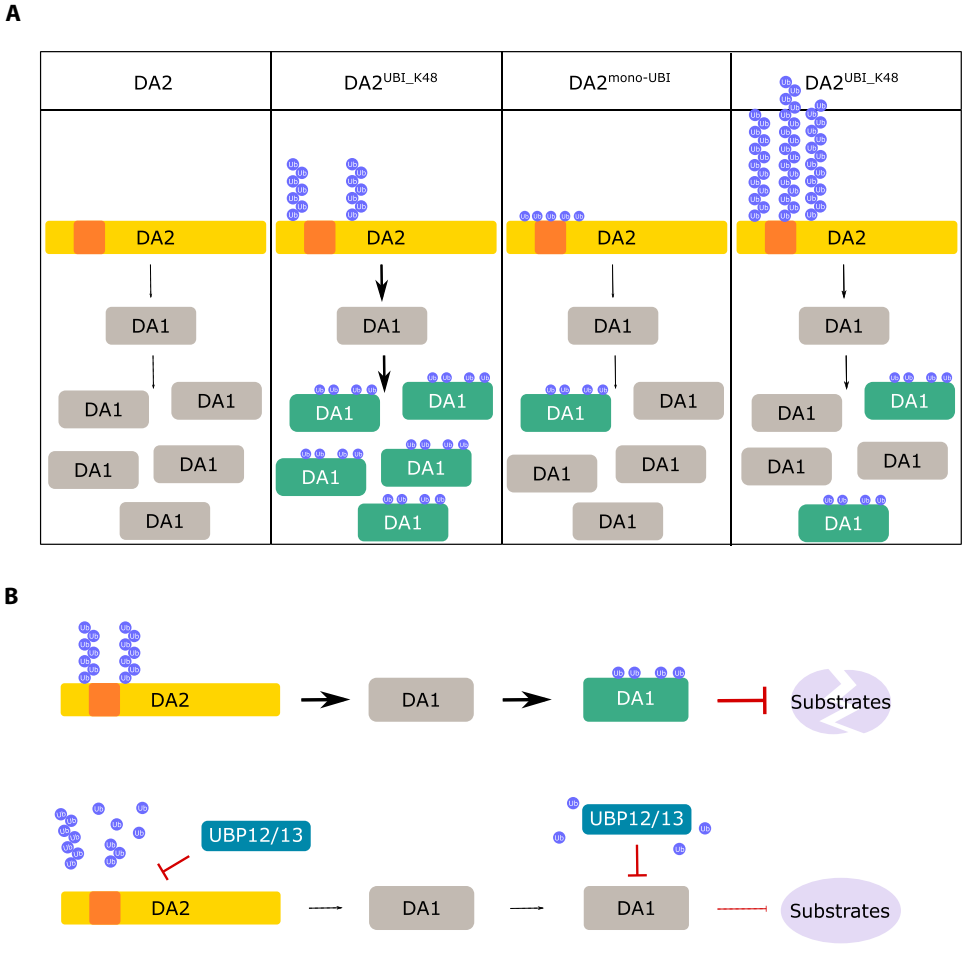

Fig. 7. Schematic overview: Auto-ubiquitination levels of DA2 regulate the protease activity of DA1. (**A**) Ubiquitin chain type and length alter the enzymatic activity of DA2 toward DA1. (**B**) UBP12 and UBP13 restrict the mode of action of the ubiquitin-activated DA1 protease by limiting the activity of DA2 and by directly deubiquitinating DA1.

which could also bind DA2 in its un-ubiquitinated form in vitro (Fig. 4, A to C). UBP12 and UBP13 have been found to participate in various plant developmental processes, including plant immunity, phytohormone signaling, nutrient response, and growth, by deubiquitinating various ubiquitinated proteins and preventing their proteasomal degradation (*43*–*49*, *85*–*88*). Our experiments show that UBP12 and UBP13 specifically eliminate polyubiquitin chains from DA2 (Fig. 4, D to F, and figs. S2C and S3B). In addition, our previous work has demonstrated that UBP12 and UBP13 also deubiquitinate DA1, DAR1, and DAR2, which are substrates of DA2, hereby limiting their peptidase activity (*50*). Because polyubiquitination of DA2 initially enhances its ubiquitination activity toward DA1, deubiquitination of DA2 by UBP12 and UBP13 can serve as an additional brake to control the levels of ubiquitinated, and hence activated, DA1 (Fig. 7B). So far, the peptidase activity of DA1 and its related proteins, DAR1 and DAR2, can be attenuated by several diverse molecular mechanisms. First, ubiquitinated DA1, DAR1, and DAR2 proteins can cleave their ubiquitinating E3 ligases in a negative feedback loop (*51*). Second, UBP12 and UBP13 can directly counteract the ubiquitination of DA1, DAR1, and DAR2, reducing their activity (*50*). Third, DA1 can be phosphorylated by BRI1, resulting in the formation of high–molecular weight complexes that are inactive, regardless of their ubiquitination status (*70*). Fourth, the E3 ligases BB (*30*) and DA2, which ubiquitinate DA1, are characterized by a high turnover. Fifth, DAR3 inhibits the activity of DA1 to repress endoreduplication (*89*). Last, by directly deubiquitinating DA2 and hereby limiting its ubiquitination activity toward DA1, UBP12 and UBP13 further limit the ubiquitination of DA1 and its related proteins (Fig. 7B). Previously, we demonstrated that strong overexpression of *UBP12* and *UBP13* leads to smaller plants that contain smaller cells and have a reduced nuclear DNA content (*50*), similar to *da1ko_dar1-1_dar2-1* mutants (*52*). On the other hand, when the expression of *UBP12* or *UBP13* is driven by a milder *UBQ10* promoter, which can finally lead to lower levels of ubiquitinated DA1, leaf size is enlarged (*49*). Combined, these regulatory layers that limit the activity of DA1 strongly suggest that keeping a precise balance of ubiquitinated DA1 is vital for plant development.

Protein fusions can trigger the proteolytic activity of DA1

PTMs, such as phosphorylation, ubiquitination, and lipidation, fundamentally affect a protein's function. Therefore, methods that create artificial mimics of PTMs provide a strong tool to further understand the function of proteins. For several PTMs, methods exist to artificially mimic the modifications. For example, PIN-FORMED 1 (PIN1) is phosphorylated at Ser^{337} and/or Thr^{340}, leading to an apical localization of PIN1. Converting these serine and threonine residues to aspartic acid mimics phosphorylation of PIN1 (*90*), resulting in a constitutive, PINOID-independent apical targeting of PIN1. In mammalians, the proto-oncogene Ras plays a key role in cell growth and needs to be lipid-modified to be biologically active (*91*). By adding chemically synthesized lipidated peptides to the C terminus of Ras, the protein becomes functionally active (*92*). Because the activity of DA1 is strictly regulated on several levels, we aimed to generate a ubiquitination mimic of DA1 that is constitutively activated, hereby overruling all levels of (de) ubiquitination control. DA1 has been demonstrated to be multi-monoubiquitinated at its C-terminal domain, near its peptidase active site. However, when these lysines are mutated, ubiquitination on alternative lysines can also lead to its activation (*51*). Strong overexpression of untagged DA1, DAR1, or DAR2 can rescue the triple mutant *da1ko_dar1-1_dar2-1* phenotype but does not lead to smaller plants in *Arabidopsis* (*52*, *66*), most likely because the activity of these proteins is strictly regulated. By fusing DUB-insensitive ubiquitin molecules ($UBI^{G75V, G76V}$) to the C terminus of DA1 (DA1-UBI_n), we could trigger its protease activity toward several substrates in vitro in the absence of DA2 (Fig. 5, B and C). In addition, overexpression of these different DA1-UBI_n fusion proteins in *Arabidopsis* not only led to a severe reduction in growth and cell division but also caused a strong increase in endoreduplication (Fig. 5, D to H). This observation is in line with previous studies, demonstrating that monoubiquitination can be mimicked by ubiquitin fusions at a terminus of a protein of interest (*93*–*95*). Although it is generally known that tagging a protein of interest with the bulky GFP moiety can alter its localization and protein-protein interactions or interfere with its function, we were taken aback that our biochemical assays demonstrated that DA1 was activated by the N-terminal GFP fusion and could cleave substrates in the absence of E3-mediated ubiquitination. However, recombinant HIS-GFP-DA1-UBI_1 proteins did not show such cleavage activity. This demonstrates that, whenever possible, the molecular characteristics and behavior of tagged proteins should be assessed carefully.

On multiple levels, the DA1 pathway and brassinosteroid signaling are tightly interconnected (*10*). BRASSINAZOLE-RESISTANT 1, a positive transcriptional regulator of brassinosteroid signaling, represses the transcription of *CUP-SHAPED COTYLEDON 2* (*CUC2)* and *CUC3* (*96*), which on their turn positively regulate the expression of *DA1* (*97*). In addition, BRI1 can negatively regulate the activity of DA1 through phosphorylation (*70*). On top of this, UBP12 and UBP13 have been shown to stabilize BES1 (*45*, *46*) and BRI1 (*44*), and the double transgenic lines $BRI1^{OE}$*_bb* and $BRI1^{OE}$*_da1-1* synergistically enhance leaf size (*98*). Therefore, it will be interesting to explore the contributions to organ size in higher-order mutants of both pathways. Although over the past years, many studies have stepwise elucidated the growth-regulating DA1 pathway, the molecular consequences for DA1 caused by monoubiquitination, leading to its activation, remain however elusive. A potential explanation is that monoubiquitination could modulate the activity of DA1 by altering its protein structure. For instance, monoubiquitination of MUCOSA-ASSOCIATED LYMPHOID TISSUE LYMPHOMA TRANSLOCATION 1 (MALT1), a key regulator of the nuclear factor κB (NF-κB) signaling pathway, promotes its dimerization and hence protease activity (*95*). The multiple monoubiquitination could, for example, induce steric interference that alters the protein structure of DA1, shifts an auto-inhibitory domain, and hence exposes its active site. Potentially, this can be mimicked by ubiquitin fusions or even by adding a bulky GFP tag. Therefore, future structural biology studies by means of x-ray crystallography could be used to explore the effect of ubiquitination on the protein structure of DA1 or artificial DA1-UBI and other fusion proteins, giving more insights into this exciting growth-regulating pathway.

MATERIALS AND METHODS

Plant material and growth conditions

The *Arabidopsis* accession Columbia (Col-0) was used for the generation of all transgenic lines and as the corresponding wild-type control. All plants were grown on plates containing half-strength Murashige and Skoog medium (MS) medium (*99*) containing 1% sucrose with a density of one plant per 4 cm^2 at 21°C under a 16-hour

day/8-hour night regime in a light intensity of approximately 75 photosynthetic active radiation. For all experiments, the seeds were stratified in the dark for two nights at 4°C before being placed in the respective growth rooms. Each quantitative experiment was performed in at least three independent biological repeats.

Plasmid construction

The 1960–base pair promoter sequence of *DA2* and the coding sequence of *DA1* were amplified and cloned by Gibson Assembly (NEB, E5510S) in the Golden Gate vectors pGGA000. The coding sequences of *Ubiquitin*, *DA2*, *DA1*, *UBP12*, and *UBP13* were similarly assembled in the Golden Gate vector pGGC0000. The coding sequence of ubiquitin was also amplified with reverse primers that contained mutations to change the two C-terminal glycines to valines ($UBI^{G75V,G76V}$), hereby abolishing cleavage by deubiquitination enzymes and cloned into pGGB000, pGGC000, pGGD000, and pGGE000. In addition, the coding sequences of *DA1*, *DA2*, *UBP12*, *UBP13*, *UBP3*, *UBP15*, *UBP24*, *UBC5*, *UBC7*, *UBC8*, *UBC11*, *UBC16*, *UBC18*, *UBC26*, *UBC27*, *UBC28*, *UBC29*, *UBC35*, and *UBC36* were cloned in the Gateway vector pDonor221. The $DA2^{C59S}$, $DA1^{H418A,H422A}$, $UBP12^{C208S}$, and $UBP13^{C207S}$ mutations were introduced by site-directed mutagenesis PCR.

The *pDA2::DA2-GUS* and *pDA2::*$DA2^{C59S}$*-GUS* expression vectors were assembled using the GoldenGateway method (*100*). First, the coding sequences were assembled using Golden Gate in pEN-L1-AG-L2, which was then recombined using Gateway in the destination vector pFAST-R01. Additional *35S::DA2* constructs were generated via Golden Gate into the destination vector pFASTR-AG. For the colocalization experiments, the coding sequences of *DA2* were cloned in the Gateway destination vector pK7WGR2 and those of *UBP12* and *UBP13* in pK7WGF2 to generate N-terminal red fluorescent protein (RFP) and GFP fusion constructs, respectively. *DA2* and $DA2^{C59S}$ were cloned in the Gateway-compatible pDEST-HIS-MBP destination vector to generate HIS-MBP-DA2 and HIS-MBP-$DA2^{C59S}$. UBP3, UBP12, UBP13, $UBP12^{C208S}$, $UBP13^{C207S}$, UBP15, UBP24, UBC8, UBC10, UBC11, UBC16, UBC17, UBC18 UBC26, UBC28, UBC29, UBC30, UBC35, and UBC36 constructs were subcloned in pDEST15 to generate GST-UBP3, GST-UBP12, GST-UBP13, GST-UBP15, GST-UBP24, GST-UBC8, GST-UBC10, GST-UBC11, GST-UBC16, GST-UBC17, GST-UBC18, GST-UBC26, GST-UBC28, GST-UBC29, GST-UBC30, GST-UBC35, and GST-UBC36 fusion proteins. The GST-UBC10 construct was provided by M. Bevan (JIC, Norwich, UK). The HIS-FLAG-DA1 and HIS-FLAG-$DA1^{H418A,H422A}$ constructs were assembled in a Golden Gate–compatible protein expression vector pDEST-RC-AG using a Golden Gate reaction. For the yeast two-hybrid assay, DA2 and GUS were cloned in pGADT7-GG using Golden Gate. UBC5, UBC7, UBC16, and UB27 were cloned into pGBT9, and the other E2 enzymes in pGBT9 were provided by A. Goossens (VIB-UGent, Belgium).

To generate a single vector that encoded the bait and prey proteins for in vivo immune precipitation experiments, we generated with Golden Gate a constitutively expressed N-terminal mCherry fusion of DA2, followed by a pGG-F-A-AarI-SacB-AarI-G-G module after the 35*S* terminator in the pGGK-A-G destination vector. After a digest with *AarI*, we inserted additional expression modules of either free GFP or N-terminal GFP fusions of UBP12 or UBP13, driven by a 35*S* promotor. Similarly, we generated ratiometric constructs that encoded both a free mCherry combined with free GFP, GFP-DA2, or GFP-$DA2^{C59S}$, all expressed by the p35*S*. In addition, we generated an N-terminal tandem fluorescent timer consisting of an sfGFP and mCherry protein, separated by a small linker as described by Zhang *et al.* (*101*). With this tandem fluorescent protein timer, we generated 35*S*::sfGFP-mCherry, 35*S*::sfGFP-mCherry-DA2, and 35*S*::sfGFP-mCherry-$DA2^{C59S}$ constructs. HA-ubiquitin fusions were cloned in a pGGK-A-G destination vector, driven by a 35*S* promotor.

Overexpression constructs of *DA1* with up to four ubiquitin molecules were generated using the GoldenGateway method (*100*). First, the coding sequences were assembled using Golden Gate in pEN-L1-AG-L2, which was then recombined using Gateway in pFAST-G02. The HIS-FLAG-DA1-UBI_1 and HIS-FLAG-$DA1^{H418A,H422A}$-UBI_1 constructs were assembled in a Golden Gate–compatible protein expression vector pDEST-RC-AG using a Golden Gate reaction. All general plasmids can be requested from https://gatewayvectors.vib.be, and the primers are listed in table S3.

Transgenic plant generation

All *Arabidopsis* plants were transformed by floral dip using *Agrobacterium tumefaciens* (PMP90 C58C1). The *pDA2::DA2-GUS* and *pDA2::*$DA2^{C59S}$*-GUS* plasmids were transformed into *da2-1* mutants, the *35S::DA2* construct into Col-0, and the *da1-1* mutant. *35S::DA1-*UBI_1, *35S::DA1-*UBI_2, *35S::DA1-*UBI_3, *and 35S::DA1-*UBI_4 constructs were transformed in Col-0 plants. For all experiments, we selected homozygous single-locus insertion lines.

Leaf measurements and cellular analysis

Leaves were dissected from the rosette and placed on a square plate containing 1% agar. The leaves were imaged, and their area was analyzed with ImageJ v1.45 [RRID:SCR_003070, National Institutes of Health (NIH); http://rsb.info.nih.gov/ij/]. For the cellular analysis, leaf samples were cleared overnight in 70% ethanol, stored in lactic acid, and mounted on a microscope slide. The total leaf blade area of cleared leaves was measured for at least eight representative leaves under a dark-field binocular microscope (MZ16, Leica). Three leaves whose size were the closest to the average leaf area of each line were chosen for further analysis. Abaxial epidermal cells in the center of the leaf blade, between the midvein and leaf edge, were drawn using a microscope equipped with differential interference contrast optics (DM LB with 403 and 633 objectives, Leica) and a drawing tube. Photographs of leaves and scanned cell drawings were used to measure leaf and individual cell area, respectively, as described before (*102*).

Flow cytometry

The first leaf pair was harvested from 9 to 21 DAS with a 3-day interval and frozen in liquid nitrogen. At least three leaves per time point of each biological repeat were chopped with a razor blade in 200 µl of Cystain UV Precise P Nuclei Extraction buffer (Sysmex), then 800 µl of Cystain UV Precise P Staining buffer (Sysmex) was added, and the solution was filtered through a 50-mm filter. Nuclei were analyzed with the Cyflow MB flow cytometer (Partec) and the FloMax software (RRID:SCR_014437).

Recombinant protein production and quantification

All expression vectors were transformed into competent BL21 (DE3) *E. coli* cells. The specific conditions for protein production are listed in table S4. HIS-MBP-DA2, MBP-TCP22-GST, and MBP-UBP15-GST were purified from the bacterial lysate with amylose resin agarose

beads (BioLabs, E8021S), DA2-GST, GST-UBP3, GST-UBP12, GST-UBP13, GST-UBP15, GST-UBP24, GST-UBC8, GST-UBC10, GST-UBC11, GST-UBC16, GST-UBC17, GST-UBC18, GST-UBC26, GST-UBC28, GST-UBC29, GST-UBC30, GST-UBC35, and GST-UBC36 with glutathione Sepharose 4B beads (GE Healthcare, 17075601). DA2-HIS, HIS-FLAG-DA1, HIS-FLAG- DA1^{H418A,H422A}, HIS-FLAG-DA1-UBI$_1$, HIS-GFP-DA1, and HIS-GFP-DA1-UBI$_1$ were purified with Ni-NTA agarose beads (QIAGEN, 30210).

Purified proteins were loaded on 4 to 15% Mini-PROTEAN TGX Precast Protein Gels (Bio-Rad, 4561083DC) and stained with Instant Blue (Sigma-Aldrich, ISB1L-1 L), and the full-length proteins were quantified using a bovine serum albumin (BSA) standard curve in ImageLab (V.6.0.1; Bio-Rad, RRID:SCR_014210).

In vitro ubiquitination and deubiquitination assays

The ubiquitination of DA2 or DA1 was carried out in 30 μl of ubiquitination buffer [50 mM tris-HCl (pH 7.4), 5 mM $MgCl_2$, 2 mM ATP, 2 mM dithiothreitol (DTT)] in the presence of 20 μg of ubiquitin [recombinant human ubiquitin protein, R&D Systems, U-100H; recombinant human HA-ubiquitin protein, R&D Systems, U-110; recombinant human ubiquitin mutant (no lysine) protein, R&D Systems, UM-NOK], 100 ng of E1 (UBE1, R&D Systems, E-305), 500 ng of E2 (UbcH5b/UBE2D2, R&D Systems, E2-622 or recombinant *Arabidopsis* E2 enzymes), 200 ng of recombinant DA2, and, if applicable, 200 ng of DA1. Before the deubiquitination step, the E1 inhibitor MLN7324 (Chemietek, CT-M7243) was added to terminate the ubiquitination reaction. Subsequently, 200 ng of full-length GST-tagged UBP proteins were added to the samples for 4 hours. The samples were loaded on 4 to 15% Mini-PROTEAN TGX Precast Protein Gels (Bio-Rad, 4561083DC). The gels were transferred to a polyvinylidene difluoride membrane using Trans-blot turbo transfer packs (Bio-Rad, 170-4156), and the membranes were incubated overnight in a 5% skimmed milk (Difco, 232100), 1× Tris-buffered saline with 0.1% Triton-X (TBST) solution. After blocking, GST-tagged proteins were detected with anti-GST horseradish peroxidase (HRP) conjugate (1:3000; Sigma-Aldrich, GERPN1236, RRID:AB_2827942), MBP-tagged proteins with anti-MBP monoclonal antibody (1:10,000; NEB, E8030S, RRID:AB_1559728), HIS-tagged proteins with anti-HIS–HRP (1:2500; GenScript, A00612) or anti-HIS (1:2000; Invitrogen, R93025), FLAG-tagged proteins with anti-Flag (1:2000; Sigma-Aldrich, F3165), and HA-tagged proteins with anti-HA–HRP (1:5000; Abcam, ab1190). For the general detection of ubiquitin, anti-P4D1 (1:2000; Santa Cruz Biotechnology, SC-8017) was used, and to determine the ubiquitin linkage type, we used anti-K48 (1:1000 in 5% BSA, Cell Signaling Technology, catalog no. 8081) and anti-K63 (1:1000; Sigma-Aldrich, catalog no. 05-1308). The α-K48 and α-K63 blots were always detected with the same exposure time. As secondary antibodies, rabbit immunoglobulin G (IgG) HRP-linked antibody (1:2000; Sigma-Aldrich, NA934v, RRID:AB_2722659) and mouse IgG HRP-linked antibody (1:5000; Sigma-Aldrich, NA931v, RRID:AB_2827944) were used. The protein blots were visualized using the chemiluminescence assay kit (Thermo Fisher Scientific, catalog no.32106) in a ChemiDoc imaging system (Bio-Rad) and further processed with ImageLab (v.6.0.1; Bio-Rad, RRID:SCR_014210).

In vitro E3 ligase ubiquitination efficiency assay

DA2-HIS was incubated with E1, E2, and ubiquitination buffer, including ATP, in the presence or absence of ubiquitin [recombinant human ubiquitin Protein, R&D Systems, U-100H; recombinant human ubiquitin mutant (no lysine) protein, R&D Systems, UM-NOK] to generate ubiquitination-modified DA2 or unmodified DA2. After 4 hours, additional ubiquitin and equal amounts of HIS-FLAG-DA1^{H418A,H422A} were added, which we considered as time point 0. Samples were harvested during a time course, and the reaction was stopped by adding 5× SDS sample buffer. The ubiquitination levels of DA2-HIS and HIS-FLAG-DA1^{H418A,H422A} were further detected by Western blot.

Yeast two-hybrid assay

Constructs were transformed into the yeast strain PJ69-4A with the Frozen-EZ Yeast Transformation II Kit (Zymo Research, T2001) according to the manufacturer's instructions. Yeast cultures were handled, and interaction assays were performed as described in the Yeast Protocols Handbook (https://takara.co.kr/file/manual/pdf/PT3024-1.pdf).

Transient expression in *N. benthamiana* and fluorescence microscopy

A 3-ml culture of *Agrobacterium* (PMP90 C58C1) containing *35S::RFP-DA2*, *35S::GFP-UBP12*, *35S::GFP-UBP13* constructs or P19 was grown overnight (28°C) in YEB medium with the appropriate antibiotics. The next day, 1 ml of this culture was inoculated in a 9-ml YEB, 10 mM MES, and 20 μM acetosyringone (Aldrich, D134406) solution with the appropriate antibiotics and incubated overnight at 28°C. Then, the bacteria were washed twice in a 100 mM $MgCl_2$, 10 mM MES, and 20 μM acetosyringone buffer, and the OD_{600} (optical density at 600 nm) was adjusted to 1 for all cultures and further incubated for 2 hours at 28°C. Then, equal mixtures of the constructs were infiltrated in leaves of 4-week-old *N. benthamiana* plants. After three nights, leaf disks were imaged with a Zeiss LSM 710 confocal inverted microscope (RRID:SCR_018063, Zeiss) to image the RFP (lasers: 561 nm: 3.0%, beam splitters: Main Beam Splitter (MBS): MBS 488/561, pinhole: 100 μm, digital gain: 1.00, Master gain: 925) and GFP fusion proteins (lasers: 488 nm: 2.0%, beam splitters: MBS_InVis: Plate, pinhole: 100 μm, digital gain: 0.75, Master gain: 956). The image overlay was generated using the Zen 2009 software (6.0 SP2, Carl Zeiss). For the study of subcellular localization of DA2, UBP12, and UBP13, images were taken by an SP8X confocal microscope (Leica) with a ×40/1.10 water objective. GFP and RFP were excited at 488 and 594 nm and acquired at 500 to 530 nm and at 600 to 650 nm, respectively. Images were collected using Las-X software (v3.5.7.23225).

Protein stability assays

To measure protein turnover in *N. benthamiana*, free GFP, GFP-DA2, or GFP-DA2^{C59S} was expressed together with the mCherry reference protein from the same vector. These vectors were transformed into *Agrobacterium* (PMP90 C58C1), and leaves were infiltrated as described above. The free GFP control construct was always infiltrated on the same leaf at the same region. After 2 days, the fluorescence was imaged at three locations per leaf using a Leica fluorescence binocular stereoscope (M165-FC, Leica) equipped with a camera (DFC-7000T, Leica), and the ratio of GFP/mCherry of each construct was calculated in ImageJ v1.45 ((RRID:SCR_003070, NIH; http://rsb.info.nih.gov/ij/). In total, at least three biological replicates were performed. sfGFP-mCherry-DA2, sfGFP-mCherry-DA2^{C59S}, and the free sfGFP-mCherry control were transformed in suspension

cells as described before (*103*). Cell suspensions were pipetted in a black, optically clear-bottom, 96-well plate (PerkinElmer, 6005225), and the fluorescence was measured in a CLARIOstar Plus (BMG Labtech) (sfGFP: excitation 470-15, emission 530-20; mCherry: excitation 572-15, emission 630-20).

Histochemical GUS staining

At 9 DAS, *pDA2::DA2-GUS* and *pDA2::DA2*^{C59S}*-GUS* seedlings were moved to liquid half-strength MS medium. BTZ was added to the medium to a final working concentration of 40 μM, and the same amount of dimethyl sulfoxide (DMSO) was added to the control group. After 24 hours of treatment, the seedlings were incubated in 80% acetone for 20 min, transferred to an X-Gluc staining solution [500 mM phosphate buffer (pH 7.0), 0.5 mM $K_3Fe(CN)_6$ (potassium ferricyanide), 0.5 mM $K_4Fe(CN)_6$ (potassium ferrocyanide), 1 mM X-Gluc (Fermentas, R0852), 0.5% dimethylformamide, 1 mM EDTA, and 0.5% Triton X-100], and incubated overnight at 37°C. Then, the samples were cleared overnight in 70% ethanol, stored in lactic acid, mounted on a microscope slide, and imaged using a dark-field binocular microscope (MZ16, Leica).

LC-MS/MS analysis of ubiquitinated DA2

For the detection of ubiquitinated lysines, 10 μg of ubiquitinated HIS-MBP-DA2 was submitted for liquid chromatography–tandem mass spectrometry (LC-MS/MS). The run was searched using the MaxQuant algorithm (version 2.0.3.0) with mainly default search settings, including a false discovery rate set at 1% on propensity score matching (PSM), peptide, and protein level. GlyGly on lysine residues was set to variable. Missed cleavages were set to maximum 3. The detailed MS/MS results can be found in table S1.

Isolation of DA2 protein complexes by AP-MS

Transgenic *Arabidopsis thaliana* cell suspension cultures expressing *GSrhino-DA2* from the constitutive 35*S* cauliflower mosaic virus promoter were generated as previously described (*103*, *104*). Cells were treated with 50 μM MG132 for 6 hours and flash-frozen in liquid nitrogen, 3 days after subculturing in fresh Murashige and Skoog basal salts with minimal organics (MSMO) medium. Protein interactions were stabilized by in vitro cross-linking with dithiobis succinimidyl propionate (DSP; Thermo Fisher Scientific, Pierce), and protein complexes were isolated in triplicate by protein G–based AP-MS, as previously described (*105*, *106*). Briefly, cells were ground in liquid nitrogen and proteins were extracted in extraction buffer [50 mM Hepes (pH 7.5), 15 mM $MgCl_2$, 150 mM NaCl, 15 mM *p*-nitrophenyl phosphate, 60 mM β-glycerophosphate, 0.1% NP-40, 0.1 mM Na_3VO_4, 1 mM NaF, 1 mM phenylmethylsulfonyl fluoride, 1 μM E64, EDTA-free Ultra cOmplete tablet (Roche), and 5% ethylene glycol]. To stabilize transient protein interactions, the proteins were cross-linked for 45 min with 3 mM DSP during protein solubilization at 4°C on an orbital shaker. Before the centrifugation of protein extracts, nonreacted DSP was quenched with 1 ml of 1 M tris-HCl buffer (pH 7.5). After centrifugation, protein complexes were trapped by incubating 25 mg of total protein extract for 2 hours with 50 μl of magnetic IgG bead suspension [prepared in-house as described by Hamperl *et al.* (*107*)]. The beads were washed three times with 500 μl of extraction buffer and once with 500 μl of extraction buffer without detergent. Next, the proteins were eluted by incubating the washed IgG beads three times with 150 μl of 0.2 M glycine/HCl (pH 2.5) at 4°C. The pooled eluate was neutralized with 100 μl $(NH_4)_2CO_3$. Proteins were reduced for 30 min in 5 mM tris(2-carboxyethyl)phosphine (TCEP) at 37°C, alkylated for 30 min in 10 mM iodoacetamide at room temperature, and digested overnight with 1 μg of trypsin/Lys-C at 37°C. Peptides were acidified to 1% (v/v) trifluoroacetic acid, desalted on C18 Omix tips (Agilent, catalog no. A57003100), dried in a SpeedVac, and stored at −20°C until MS analysis. The peptide samples were analyzed on a Q Exactive (Thermo Fisher Scientific), and copurified proteins were identified with Mascot (version 2.5.1, Matrix Science) using standard procedures (*104*, *105*). Briefly, the raw data were searched against the TAIRplus database [35839 entries, (*104*)]. Variable modifications were set to methionine oxidation and acetylation of protein N termini. Fixed modifications were set to carbamidomethylation of cysteines. Precursor mass tolerance was set to 10 parts per million (with Mascot's C13 option set to 1) and the fragment mass tolerance to 20 milli mass unit (mmu). Peptide charges were set to 2+ and 3+ and the instrument to ESI-QUAD. Protease was set to trypsin/P, allowing for two missed cleavages. Significance threshold was set to $P < 0.01$, and ion score cutoff to <0.01 (table S2A). After identification, the obtained protein list was filtered versus a large dataset of pull-downs with nonrelated baits, assembled similarly as described (table S2B) (*104*). The identified proteins were retained by means of semiquantitative analysis using the average normalized spectral abundance factors (NSAFs) of the identified proteins in the bait pull-downs versus the average NSAF of the same identified protein in the large dataset. In the same way, the list of identified proteins was additionally filtered versus a dataset containing only DSP cross-linked samples. Proteins identified with one peptide in at least two experiments, showing high (at least 10-fold) and significant $\{-\log_{10}[P \text{ value}(t \text{ test})] \geq 8\}$ enrichment compared to the calculated average NSAF values from the large dataset of pull-downs as well as the DSP cross-linked dataset, were retained. All protein identification details can be found in table S2.

In vivo Co-IP

Vectors that simultaneously carried constructs of free GFP, GFP-UBP12, or GFP-UBP13 with mCherry-DA2 were transformed in cell suspension cultures, and the protein extraction was performed as described by Van Leene *et al.* (*103*). Proteins were extracted and purified with GFP-Trap Agarose beads (ChromoTek, RRID:AB_2631357), and the purified fractions were subjected to Western blot. After blocking, GFP-tagged proteins were detected with anti-GFP antibody (1:1000; Abcam, ab290, RRID:AB_303395) and mCherry-tagged proteins with anti-RFP antibody (1:1000; ChromoTek, RFP antibody [6G6], RRID:AB_2631395) and subsequently with a secondary rabbit IgG HRP-linked antibody (1:2000; Sigma-Aldrich, NA934v, RRID:AB_2722659) or secondary mouse IgG HRP-linked antibody (1:5000; Sigma-Aldrich, NA931v, RRID:AB_2827944), respectively. The protein blots were visualized as described in the previous section.

In vitro pull-down

For the in vitro pull-down assays of DA2 by UBP12 or UBP13, around 2 μg of GST-UBP12, GST-UBP13, or GST proteins was incubated with 5 μg of HIS-MBP-DA2 protein in 1 ml of pull-down buffer [10% glycerol, 1% Triton X-100, 150 mM NaCl, 50 mM Hepes (pH 7.5), and 1× cOmplete protease inhibitor cocktail (Roche, 11697498001)]. These reactions were incubated with 15 μl of GST beads (glutathione Sepharose 4B agarose) while gently shaking at 4°C for 1 hour. The beads were washed six times, and the proteins were eluted with 35 μl of GST elution buffer [50 mM tris-HCl (pH 8.0), 10 mM

reduced glutathione, and 10% glycerol] for 30 min at 4°C. The eluted samples were heated for 10 min at 95°C after the addition of 5× sample buffer. The immunoprecipitated proteins were separated by SDS–polyacrylamide gel electrophoresis and detected with anti-GST HRP conjugate (1:3000; Sigma-Aldrich, GERPN1236, RRID:AB_2827942) and MBP-tagged proteins with anti-MBP monoclonal antibody (1:10,000; NEB, E8030S, RRID:AB_1559728) and subsequently with a secondary mouse IgG HRP-linked antibody (1:5000; Sigma-Aldrich, NA931v, RRID:AB_2827944). The protein blots were visualized as described in the previous section.

Cell-free ubiquitination assay

Proteins were freshly extracted from 8-day-old seedlings of Col-0, *ubp12-2*, *35S::UBP12*, and *35S::UBP13* using a 0.5 M sucrose, 1 mM $MgCl_2$, 10 mM EDTA (pH 8.0), 5 mM DTT, and 50 mM tris-MES (pH 8.0) extraction buffer without protease inhibitors (1 μl of buffer was added per milligram of plant material). Subsequently, 600 μg of cell-free extract was added per 200 ng of HIS-MBP-DA2 proteins, and MG132 was supplemented to a final concentration of 50 μM. For each time point, an equal amount (30 μl) of reaction mix was taken and the reaction was stopped by the addition of SDS sample buffer. The samples were blotted and detected as described above. The intensities of ubiquitinated HIS-MBP-DA2 were measured in ImageJ. To quantify the ubiquitination, relative ubiquitination intensities were calculated as ubiquitination intensities at 2 hours compared to the background signal at 0 hours.

In vivo ubiquitination assay in *Arabidopsis* protoplasts

Protoplasts of 14-day-old seedlings of *Arabidopsis* were isolated as described by Zhai *et al*. (*108*). Expression vector plasmids of *35S::HA-ubiquitin*, *35S::sfGFP-mCherry-DA2*, *35S::sfGFP-mCherry-DA2*^{C59S},*35S::mCherry-DA2*,*35S::GFP-UBP12*,*35S::GFP-UBP12*^{C208S}, *35S::GFP-UBP13*, and *35S::GFP-UBP13*^{C207S} were prepared with a QIAGEN Plasmid Maxi Kit (QIAGEN, 12163) according to the manufacturer's instructions. In total, 200 μl of plasmids at the concentration of 1000 ng/μl were transfected into protoplasts. These protoplasts were incubated overnight at 21°C. Then, BTZ was added to the medium to a final working concentration of 5 μM, and the same amount of DMSO was added to the control group. After 6 hours of treatment, the protoplasts were harvested and the proteins were extracted as described before. After purification with GFP-Trap agarose beads (ChromoTek, RRID:AB_2631357) or ChromoTek RFP-Trap Magnetic Agarose beads (ChromoTek, RRID:AB_2631363), the purified DA2 proteins were further analyzed by Western blot. The intensities of BTZ-treated ubiquitinated sfGFP-mCherry-DA2 and sfGFP-mCherry-DA2^{C59S} were measured in ImageJ. To quantify the ubiquitination, relative ubiquitination intensities in the α-HA, α-P4D1, and α-K48 blots were normalized to the abundance of the respective unmodified protein in the α-GFP blot.

In vitro DA1-mediated cleavage assays

HIS-FLAG-DA1^{UB} and HIS-FLAG-DA1$^{H418A,H422A\ UB}$ were generated in vitro using HIS-MBP-DA2 as E3 ligases. Nine hundred nanograms of HIS-FLAG-DA1, HIS-FLAG-DA1^{UB}, HIS-FLAG-DA1$^{H418A,H422A\ UB}$, HIS-FLAG-DA1-UBI_1, HIS-FLAG-DA1^{H418A,H422A}-UBI_1, HIS-GFP-DA1, or HIS-GFP-DA1-UBI_1 was added to 200 ng of MBP-UBP15-GST or MBP-TCP22-GST in a 60-μl reaction in ubiquitination buffer. Reactions were carried out for 6 hours at 30°C and terminated by the addition of SDS sample buffer.

RNA extraction, cDNA preparation, and qRT-PCR

Total RNA was extracted from flash-frozen seedlings. To eliminate the residual genomic DNA present in the preparation, the RNA was treated by RQ1 ribonuclease-free deoxyribonuclease according to the manufacturer's instructions (Promega, M6101) and purified with the RNeasy Mini Kit (QIAGEN, 74904). Complementary DNA (cDNA) was made with a QScript cDNA supermix kit (Quantabio, 95048-100) according to the manufacturer's instructions. qRT-PCR was done on LightCycler 480 (Roche) in 384-well plates with LightCycler 480 SYBR Green I Master Mix (Roche) according to the manufacturer's instructions. Primers were designed with Primer3 (RRID:SCR_003139, http://primer3.ut.ee). Data analysis was performed using the ΔΔCT method (*109*), taking the primer efficiency into account. The expression values were normalized using three reference genes (AT1G13320, AT2G32170, and AT2G28390) according to the GeNorm algorithm (*110*). The qRT-PCR primers are listed table S3.

Statistical analysis

Statistical parameters are indicated in the legends of each figure. The details and output of each statistical test are provided together with the source data in the corresponding source data files. A *P* value of less than 0.05 was considered significant. All statistical analysis and graphs were performed in GraphPad Prism 9. 4 (www.graphpad.com, RRID:SCR_002798).

Supplementary Materials

This PDF file includes:

Figs. S1 to S7
Legends for tables S1 to S4
Legend for source data

Other Supplementary Material for this manuscript includes the following:

Tables S1 to S4
Source data

REFERENCES AND NOTES

1. T. Hander, Á. D. Fernández-Fernández, R. P. Kumpf, P. Willems, H. Schatowitz, D. Rombaut, A. Staes, J. Nolf, R. Pottie, P. Yao, A. Gonçalves, B. Pavie, T. Boller, K. Gevaert, F. Van Breusegem, B. Sebastian, S. Stael, Damage on plants activates Ca^{2+}-dependent metacaspases for release of immunomodulatory peptides. *Science* **363**, eaar7486 (2019).
2. Á. Eseverri, C. Baysal, V. Medina, T. Capell, P. Christou, L. M. Rubio, E. Caro, Transit peptides from photosynthesis-related proteins mediate import of a marker protein into different plastid types and within different species. *Front. Plant Sci.* **11**, 560701 (2020).
3. B. Gu, H. Dong, C. Smith, G. Cui, Y. Li, M. W. Bevan, Modulation of receptor-like transmembrane kinase 1 nuclear localization by DA1 peptidases in *Arabidopsis*. *Proc. Natl. Acad. Sci. U.S.A.* **119**, e2205757119 (2022).
4. M. J. Holdsworth, J. Vicente, G. Sharma, M. Abbas, A. Zubrycka, The plant N-degron pathways of ubiquitin-mediated proteolysis. *J. Integr. Plant Biol.* **62**, 70–89 (2020).
5. R. D. Vierstra, The ubiquitin–26S proteasome system at the nexus of plant biology. *Nat. Rev. Mol. Cell Biol.* **10**, 385–397 (2009).
6. A. Sadanandom, M. Bailey, R. Ewan, J. Lee, S. Nelis, The ubiquitin-proteasome system: Central modifier of plant signalling. *New Phytol.* **196**, 13–28 (2012).
7. R. M. Vaughan, A. Kupai, S. B. Rothbart, Chromatin regulation through ubiquitin and ubiquitin-like histone modifications. *Trends Biochem. Sci.* **46**, 258–269 (2021).
8. L. Sun, Z. J. Chen, The novel functions of ubiquitination in signaling. *Curr. Opin. Cell Biol.* **16**, 119–126 (2004).
9. R. C. Aguilar, B. Wendland, Ubiquitin: Not just for proteasomes anymore. *Curr. Opin. Cell Biol.* **15**, 184–190 (2003).
10. Y. Chen, D. Inzé, H. Vanhaeren, Post-translational modifications regulate the activity of the growth-restricting protease DA1. *J. Exp. Bot.* **72**, 3352–3366 (2021).
11. J. Callis, The ubiquitination machinery of the ubiquitin system. *Arabidopsis Book* **12**, e0174 (2014).

12. X. Ma, C. Zhang, D. Y. Kim, Y. Huang, E. Chatt, P. He, R. D. Vierstra, L. Shan, Ubiquitylome analysis reveals a central role for the ubiquitin-proteasome system in plant innate immunity. *Plant Physiol.* **185**, 1943–1965 (2021).
13. Y. T. Kwon, A. Ciechanover, The ubiquitin code in the ubiquitin-proteasome system and autophagy. *Trends Biochem. Sci.* **42**, 873–886 (2017).
14. J. S. Thrower, L. Hoffman, M. Rechsteiner, C. M. Pickart, Recognition of the polyubiquitin proteolytic signal. *EMBO J.* **19**, 94–102 (2000).
15. M. L. Matsumoto, K. E. Wickliffe, K. C. Dong, C. Yu, I. Bosanac, D. Bustos, L. Phu, D. S. Kirkpatrick, S. G. Hymowitz, M. Rape, R. F. Kelley, V. M. Dixit, K11-linked polyubiquitination in cell cycle control revealed by a K11 linkage-specific antibody. *Mol. Cell* **39**, 477–484 (2010).
16. P. Liu, W. Gan, S. Su, A. V. Hauenstein, T.-M. Fu, B. Brasher, C. Schwerdtfeger, A. C. Liang, M. Xu, W. Wei, K63-linked polyubiquitin chains bind to DNA to facilitate DNA damage repair. *Sci. Signal.* **11**, eaar8133 (2018).
17. M. Tao, P. C. Scacheri, J. M. Marinis, E. W. Harhaj, L. E. Matesic, D. W. Abbott, ITCH K63-ubiquitinates the NOD2 binding protein, RIP2, to influence inflammatory signaling pathways. *Curr. Biol.* **19**, 1255–1263 (2009).
18. N. Romero-Barrios, G. Vert, Proteasome-independent functions of lysine-63 polyubiquitination in plants. *New Phytol.* **217**, 995–1011 (2018).
19. R. Yau, M. Rape, The increasing complexity of the ubiquitin code. *Nat. Cell Biol.* **18**, 579–586 (2016).
20. M. D. Stewart, T. Ritterhoff, R. E. Klevit, P. S. Brzovic, E2 enzymes: More than just middle men. *Cell Res.* **26**, 423–440 (2016).
21. C. Brillada, M. Trujillo, E2 ubiquitin-conjugating enzymes (UBCs): Drivers of ubiquitin signalling in plants. *Essays Biochem.* **66**, 99–110 (2022).
22. T. Wu, Y. Merbl, Y. Huo, J. L. Gallop, A. Tzur, M. W. Kirschner, UBE2S drives elongation of K11-linked ubiquitin chains by the Anaphase-Promoting Complex. *Proc. Natl. Acad. Sci. U.S.A.* **107**, 1355–1360 (2010).
23. S. Wang, L. Cao, H. Wang, *Arabidopsis* ubiquitin-conjugating enzyme UBC22 is required for female gametophyte development and likely involved in Lys^{11}-linked ubiquitination. *J. Exp. Bot.* **67**, 3277–3288 (2016).
24. Q. Zhao, M. Tian, Q. Li, F. Cui, L. Liu, B. Yin, Q. Xie, A plant-specific in vitro ubiquitnation analysis system. *Plant J.* **74**, 524–533 (2013).
25. W. Li, M. H. Bengtson, A. Ulbrich, A. Matsuda, V. A. Reddy, A. Orth, S. K. Chanda, S. Batalov, C. A. P. Joazeiro, Genome-wide and functional annotation of human E3 ubiquitin ligases identifies MULAN, a mitochondrial E3 that regulates the organelle's dynamics and signaling. *PLOS ONE* **3**, e1487 (2008).
26. L. Buetow, D. T. Huang, Structural insights into the catalysis and regulation of E3 ubiquitin ligases. *Nat. Rev. Mol. Cell Biol.* **17**, 626–642 (2016).
27. K. L. Lorick, J. P. Jensen, S. Fang, A. M. Ong, S. Hatakeyama, A. M. Weissman, RING fingers mediate ubiquitin-conjugating enzyme (E2)-dependent ubiquitination. *Proc. Natl. Acad. Sci. U.S.A.* **96**, 11364–11369 (1999).
28. Y. Amemiya, P. Azmi, A. Seth, Autoubiquitination of BCA2 RING E3 ligase regulates its own stability and affects cell migration. *Mol. Cancer Res.* **6**, 1385–1396 (2008).
29. H. Liu, S. L. Stone, Abscisic acid increases *Arabidopsis* ABI5 transcription factor levels by promoting KEG E3 ligase self-ubiquitination and proteasomal degradation. *Plant Cell* **22**, 2630–2641 (2010).
30. S. Disch, E. Anastasiou, V. K. Sharma, T. Laux, J. C. Fletcher, M. Lenhard, The E3 ubiquitin ligase BIG BROTHER controls *Arabidopsis* organ size in a dosage-dependent manner. *Curr. Biol.* **16**, 272–279 (2006).
31. E. Isono, M.-K. Nagel, Deubiquitylating enzymes and their emerging role in plant biology. *Front. Plant Sci.* **5**, 56 (2014).
32. J. Michael, The emerging roles of deubiquitinases in plant proteostasis. *Essays Biochem.* **66**, 147–154 (2022).
33. R. Luo, K. Yang, W. Xiao, Plant deubiquitinases: From structure and activity to biological functions. *Plant Cell Rep.* **42**, 469–486 (2023).
34. F. E. Reyes-Turcu, K. H. Ventii, K. D. Wilkinson, Regulation and cellular roles of ubiquitin-specific deubiquitinating enzymes. *Annu. Rev. Biochem.* **78**, 363–397 (2009).
35. E. March, S. Farrona, Plant deubiquitinases and their role in the control of gene expression through modification of histones. *Front. Plant Sci.* **8**, 2274 (2018).
36. P. Majumdar, U. Nath, De-ubiquitinases on the move: An emerging field in plant biology. *Plant Biol.* **22**, 563–572 (2020).
37. M. J. Skelly, J. J. Furniss, H. Grey, K.-W. Wong, S. H. Spoel, Dynamic ubiquitination determines transcriptional activity of the plant immune coactivator NPR1. *eLife* **8**, e47005 (2019).
38. Y. Xu, W. Jin, N. Li, W. Zhang, C. Liu, C. Li, Y. Li, UBIQUITIN-SPECIFIC PROTEASE14 interacts with ULTRAVIOLET-B INSENSITIVE4 to regulate endoreduplication and cell and organ growth in *Arabidopsis*. *Plant Cell* **28**, 1200–1214 (2016).
39. S. Jiang, B. Meng, Y. Zhang, N. Li, L. Zhou, X. Zhang, R. Xu, S. Guo, C.-P. Song, Y. Li, An SNW/SKI-INTERACTING PROTEIN influences endoreduplication and cell growth in *Arabidopsis*. *Plant Physiol.* **190**, 2217–2228 (2022).
40. L. Du, N. Li, L. Chen, Y. Xu, Y. Li, Y. Zhang, C. Li, Y. Li, The ubiquitin receptor DA1 regulates seed and organ size by modulating the stability of the ubiquitin-specific protease UBP15/SOD2 in *Arabidopsis*. *Plant Cell* **26**, 665–677 (2014).
41. Y. Liu, F. Wang, H. Zhang, H. He, L. Ma, X. W. Deng, Functional characterization of the *Arabidopsis ubiquitin-specific protease* gene family reveals specific role and redundancy of individual members in development. *Plant J.* **55**, 844–856 (2008).
42. R. Ewan, R. Pangestuti, S. Thornber, A. Craig, C. Carr, L. O'Donnell, C. Zhang, A. Sadanandom, Deubiquitinating enzymes AtUBP12 and AtUBP13 and their tobacco homologue NtUBP12 are negative regulators of plant immunity. *New Phytol.* **191**, 92–106 (2011).
43. J. S. Jeong, C. Jung, J. S. Seo, J.-K. Kim, N.-H. Chua, The deubiquitinating enzymes UBP12 and UBP13 positively regulate MYC2 levels in jasmonate responses. *Plant Cell* **29**, 1406–1424 (2017).
44. Y. Luo, J. Takagi, L. A. N. Claus, C. Zhang, S. Yasuda, Y. Hasegawa, J. Yamaguchi, L. Shan, E. Russinova, T. Sato, Deubiquitinating enzymes UBP12 and UBP13 stabilize the brassinosteroid receptor BRI1. *EMBO Rep.* **23**, e53354 (2022).
45. J. Xiong, F. Yang, X. Yao, Y. Zhao, Y. Wen, H. Lin, H. Guo, Y. Yin, D. Zhang, The deubiquitinating enzymes UBP12 and UBP13 positively regulate recovery after carbon starvation by modulating BES1 stability in *Arabidopsis thaliana*. *Plant Cell* **34**, 4516–4530 (2022).
46. S.-H. Park, J. S. Jeong, Y. Zhou, N. F. Binte Mustafa, N.-H. Chua, Deubiquitination of BES1 by UBP12/UBP13 promotes brassinosteroid signaling and plant growth. *Plant Commun.* **3**, 100348 (2022).
47. G. Liu, J. Liang, L. Lou, M. Tian, X. Zhang, L. Liu, Q. Zhao, R. Xia, Y. Wu, Q. Xie, F. Yu, The deubiquitinases UBP12 and UBP13 integrate with the E3 ubiquitin ligase XBAT35. 2 to modulate VPS23A stability in ABA signaling. *Sci. Adv.* **8**, eabl5765 (2022).
48. Z. An, Y. Liu, Y. Ou, J. Li, B. Zhang, D. Sun, Y. Sun, W. Tang, Regulation of the stability of RGF1 receptor by the ubiquitin-specific proteases UBP12/UBP13 is critical for root meristem maintenance. *Proc. Natl. Acad. Sci. U.S.A.* **115**, 1123–1128 (2018).
49. S.-H. Park, J. S. Jeong, J. S. Seo, B. S. Park, N.-H. Chua, *Arabidopsis* ubiquitin-specific proteases UBP12 and UBP13 shape ORE1 levels during leaf senescence induced by nitrogen deficiency. *New Phytol.* **223**, 1447–1460 (2019).
50. H. Vanhaeren, Y. Chen, M. Vermeersch, L. De Milde, V. De Vleeschhauwer, A. Natran, G. Persiau, D. Eeckhout, G. De Jaeger, K. Gevaert, D. Inzé, UBP12 and UBP13 negatively regulate the activity of the ubiquitin-dependent peptidases DA1, DAR1 and DAR2. *eLife* **9**, e52276 (2020).
51. H. Dong, J. Dumenil, F.-H. Lu, L. Na, H. Vanhaeren, C. Naumann, M. Klecker, R. Prior, C. Smith, N. McKenzie, G. Saalbach, L. Chen, T. Xia, N. Gonzalez, M. Seguela, D. Inzé, N. Dissmeyer, Y. Li, M. W. Bevan, Ubiquitylation activates a peptidase that promotes cleavage and destabilization of its activating E3 ligases and diverse growth regulatory proteins to limit cell proliferation in *Arabidopsis*. *Genes Dev.* **31**, 197–208 (2017).
52. Y. Peng, L. Chen, Y. Lu, Y. Wu, J. Dumenil, Z. Zhu, M. W. Bevan, Y. Li, The ubiquitin receptors DA1, DAR1, and DAR2 redundantly regulate endoreduplication by modulating the stability of TCP14/15 in *Arabidopsis*. *Plant Cell* **27**, 649–662 (2015).
53. T. Xia, N. Li, J. Dumenil, J. Li, A. Kamenski, M. W. Bevan, F. Gao, Y. Li, The ubiquitin receptor DA1 interacts with the E3 ubiquitin ligase DA2 to regulate seed and organ size in *Arabidopsis*. *Plant Cell* **25**, 3347–3359 (2013).
54. Q. Li, L. Li, X. Yang, M. L. Warburton, G. Bai, J. Dai, J. Li, J. Yan, Relationship, evolutionary fate and function of two maize co-orthologs of rice *GW2* associated with kernel size and weight. *BMC Plant Biol.* **10**, 143 (2010).
55. Z. Su, C. Hao, L. Wang, Y. Dong, X. Zhang, Identification and development of a functional marker of *TaGW2* associated with grain weight in bread wheat (*Triticum aestivum* L.). *Theor. Appl. Genet.* **122**, 211–223 (2011).
56. J. Bednarek, A. Boulaflous, C. Girousse, C. Ravel, C. Tassy, P. Barret, M. F. Bouzidi, S. Mouzeyar, Down-regulation of the *TaGW2* gene by RNA interference results in decreased grain size and weight in wheat. *J. Exp. Bot.* **63**, 5945–5955 (2012).
57. B. S. Choi, Y. J. Kim, K. Markkandan, Y. J. Koo, J. T. Song, H. S. Seo, GW2 functions as an E3 ubiquitin ligase for rice expansin-like 1. *Int. J. Mol. Sci.* **19**, 1904 (2018).
58. J. Hao, D. Wang, Y. Wu, K. Huang, P. Duan, N. Li, R. Xu, D. Zeng, G. Dong, B. Zhang, L. Zhang, D. Inzé, Q. Qian, Y. Li, The GW2-WG1-OsbZIP47 pathway controls grain size and weight in rice. *Mol. Plant* **14**, 1266–1280 (2021).
59. X.-J. Song, W. Huang, M. Shi, M.-Z. Zhu, H.-X. Lin, A QTL for rice grain width and weight encodes a previously unknown RING-type E3 ubiquitin ligase. *Nat. Genet.* **39**, 623–630 (2007).
60. N. Gonzalez, H. Vanhaeren, D. Inzé, Leaf size control: Complex coordination of cell division and expansion. *Trends Plant Sci.* **17**, 332–340 (2012).
61. I. Turek, N. Tischer, R. Lassig, M. Trujillo, Multi-tiered pairing selectivity between E2 ubiquitin-conjugating enzymes and E3 ligases. *J. Biol. Chem.* **293**, 16324–16336 (2018).
62. H. Zhang, E. Linster, L. Gannon, W. Leemhuis, C. A. Rundle, F. L. Theodoulou, M. Wirtz, Tandem fluorescent protein timers for noninvasive relative protein lifetime measurement in plants. *Plant Physiol.* **180**, 718–731 (2019).
63. R. S. Ranaweera, X. Yang, Auto-ubiquitination of Mdm2 enhances its substrate ubiquitin ligase activity. *J. Biol. Chem.* **288**, 18939–18946 (2013).

64. X. Cui, F. Lu, Y. Li, Y. Xue, Y. Kang, S. Zhang, Q. Qiu, X. Cui, S. Zheng, B. Liu, X. Xu, X. Cao, Ubiquitin-specific proteases UBP12 and UBP13 act in circadian clock and photoperiodic flowering regulation in *Arabidopsis*. *Plant Physiol.* **162**, 897–906 (2013).
65. N. Yan, J. H. Doelling, T. G. Falbel, A. M. Durski, R. D. Vierstra, The ubiquitin-specific protease family from *Arabidopsis*. *At*UBP1 and 2 are required for the resistance to the amino acid analog canavanine. *Plant Physiol.* **124**, 1828–1843 (2000).
66. H. Vanhaeren, Y.-J. Nam, L. De Milde, E. Chae, V. Storme, D. Weigel, N. Gonzalez, D. Inzé, Forever young: The role of ubiquitin receptor DA1 and E3 ligase Big Brother in controlling leaf growth and development. *Plant Physiol.* **173**, 1269–1282 (2017).
67. U. Hoecker, The activities of the E3 ubiquitin ligase COP1/SPA, a key repressor in light signaling. *Curr. Opin. Plant Biol.* **37**, 63–69 (2017).
68. J. Ponnu, U. Hoecker, Illuminating the COP1/SPA ubiquitin ligase: Fresh insights into its structure and functions during plant photomorphogenesis. *Front. Plant Sci.* **12**, 662793 (2021).
69. Y. Li, L. Zheng, F. Corke, C. Smith, M. W. Bevan, Control of final seed and organ size by the *DA1* gene family in *Arabidopsis thaliana*. *Genes Dev.* **22**, 1331–1336 (2008).
70. D. Hui, S. Caroline, P. Rachel, C. Ross, D. Jack, S. Gerhard, M. Neil, B. Michael, The receptor kinase BRI1 promotes cell proliferation in *Arabidopsis* by phosphorylation- mediated inhibition of the growth repressing peptidase DA1. bioRxiv 2020.05.15.098178 [Preprint] (2020). https://biorxiv.org/content/10.1101/2020.05.15.098178v2.abstract.
71. Y. Han, J. Sun, J. Yang, Z. Tan, J. Luo, D. Lu, Reconstitution of the plant ubiquitination cascade in bacteria using a synthetic biology approach. *Plant J.* **91**, 766–776 (2017).
72. N. Romero-Barrios, D. Monachello, U. Dolde, A. Wong, H. San Clemente, A. Cayrel, A. Johnson, C. Lurin, G. Vert, Advanced cataloging of lysine-63 polyubiquitin networks by genomic, interactome, and sensor-based proteomic analyses. *Plant Cell* **32**, 123–138 (2020).
73. E. Kraft, S. L. Stone, L. Ma, N. Su, Y. Gao, O.-S. Lau, X.-W. Deng, J. Callis, Genome analysis and functional characterization of the E2 and RING-type E3 ligase ubiquitination enzymes of *Arabidopsis*. *Plant Physiol.* **139**, 1597–1611 (2005).
74. P. de Bie, A. Ciechanover, Ubiquitination of E3 ligases: Self-regulation of the ubiquitin system via proteolytic and non-proteolytic mechanisms. *Cell Death Differ.* **18**, 1393–1402 (2011).
75. S.-S. Lin, R. Martin, S. Mongrand, S. Vandenabeele, K.-C. Chen, I.-C. Jang, N.-H. Chua, RING1 E3 ligase localizes to plasma membrane lipid rafts to trigger FB1-induced programmed cell death in *Arabidopsis*. *Plant J.* **56**, 550–561 (2008).
76. D.-Q. Li, K. Ohshiro, S. D. N. Reddy, S. B. Pakala, M.-H. Lee, Y. Zhang, S. K. Rayala, R. Kumar, E3 ubiquitin ligase COP1 regulates the stability and functions of MTA1. *Proc. Natl. Acad. Sci. U.S.A.* **106**, 17493–17498 (2009).
77. L. K. Linares, R. Kiernan, R. Triboulet, C. Chable-Bessia, D. Latreille, O. Cuvier, M. Lacroix, L. Le Cam, O. Coux, M. Benkirane, Intrinsic ubiquitination activity of PCAF controls the stability of the oncoprotein Hdm2. *Nat. Cell Biol.* **9**, 331–338 (2007).
78. A. Paluda, A. J. Middleton, C. Rossig, P. D. Mace, C. L. Day, Ubiquitin and a charged loop regulate the ubiquitin E3 ligase activity of Ark2C. *Nat. Commun.* **13**, 1181 (2022).
79. B. Lamothe, A. Besse, A. D. Campos, W. K. Webster, H. Wu, B. G. Darnay, Site-specific lys-63-linked tumor necrosis factor receptor-associated factor 6 auto-ubiquitination is a critical determinant of IκB kinase activation. *J. Biol. Chem.* **282**, 4102–4112 (2007).
80. Y. Herman-Bachinsky, H.-D. Ryoo, A. Ciechanover, H. Gonen, Regulation of the *Drosophila* ubiquitin ligase DIAP1 is mediated via several distinct ubiquitin system pathways. *Cell Death Differ.* **14**, 861–871 (2007).
81. K. Flick, I. Ouni, J. A. Wohlschlegel, C. Capati, W. H. McDonald, J. R. Yates, P. Kaiser, Proteolysis-independent regulation of the transcription factor Met4 by a single lys-48-linked ubiquitin chain. *Nat. Cell Biol.* **6**, 634–641 (2004).
82. K. Flick, S. Raasi, H. Zhang, J. L. Yen, P. Kaiser, A ubiquitin-interacting motif protects polyubiquitinated Met4 from degradation by the 26S proteasome. *Nat. Cell Biol.* **8**, 509–515 (2006).
83. R. Ben-Saadon, D. Zaaroor, T. Ziv, A. Ciechanover, The polycomb protein Ring1B generates self atypical mixed ubiquitin chains required for its in vitro histone H2A ligase activity. *Mol. Cell* **24**, 701–711 (2006).
84. R. Cao, Y.-I. Tsukada, Y. Zhang, Role of Bmi-1 and Ring1A in H2A ubiquitylation and Hox gene silencing. *Mol. Cell* **20**, 845–854 (2005).
85. C.-M. Lee, M.-W. Li, A. Feke, W. Liu, A. M. Saffer, J. M. Gendron, GIGANTEA recruits the UBP12 and UBP13 deubiquitylases to regulate accumulation of the ZTL photoreceptor complex. *Nat. Commun.* **10**, 3750 (2019).
86. Y. Zhou, S.-H. Park, M. Y. Soh, N.-H. Chua, Ubiquitin-specific proteases UBP12 and UBP13 promote shade avoidance response by enhancing PIF7 stability. *Proc. Natl. Acad. Sci. U.S.A.* **118**, e2103633118 (2021).
87. L. N. Lindbäck, Y. Hu, A. Ackermann, O. Artz, U. V. Pedmale, UBP12 and UBP13 deubiquitinases destabilize the CRY2 blue light receptor to regulate *Arabidopsis* growth. *Curr. Biol.* **32**, 3221–3231.e6 (2022).
88. Y. Zhou, S.-H. Park, N.-H. Chua, UBP12/UBP13-mediated deubiquitination of salicylic acid receptor NPR3 suppresses plant immunity. *Mol. Plant* **16**, 232–244 (2023).
89. B. Gu, T. Parkes, F. Rabanal, C. Smith, F.-H. Lu, N. McKenzie, H. Dong, D. Weigel, J. D. G. Jones, V. Cevik, M. W. Bevan, The integrated LIM-peptidase domain of the CSA1-CHS3/DAR4 paired immune receptor detects changes in DA1 peptidase inhibitors in *Arabidopsis*. *Cell Host Microbe* **31**, 949–961.e5 (2023).
90. J. Zhang, T. Nodzyński, A. Pěnčík, J. Rolčík, J. Friml, PIN phosphorylation is sufficient to mediate PIN polarity and direct auxin transport. *Proc. Natl. Acad. Sci. U.S.A.* **107**, 918–922 (2010).
91. M. H. Gelb, Protein prenylation, et cetera—Signal transduction in two dimensions. *Science* **275**, 1750–1751 (1997).
92. B. Bader, K. Kuhn, D. J. Owen, H. Waldmann, A. Wittinghofer, J. Kuhlmann, Bioorganic synthesis of lipid-modified proteins for the study of signal transduction. *Nature* **403**, 223–226 (2000).
93. J. Terrell, S. Shih, R. Dunn, L. Hicke, A function for monoubiquitination in the internalization of a G protein–coupled receptor. *Mol. Cell* **1**, 193–202 (1998).
94. D. Hoeller, N. Crosetto, B. Blagoev, C. Raiborg, R. Tikkanen, S. Wagner, K. Kowanetz, R. Breitling, M. Mann, H. Stenmark, I. Dikic, Regulation of ubiquitin-binding proteins by monoubiquitination. *Nat. Cell Biol.* **8**, 163–169 (2006).
95. C. Pelzer, K. Cabalzar, A. Wolf, M. Gonzalez, G. Lenz, M. Thome, The protease activity of the paracaspase MALT1 is controlled by monoubiquitination. *Nat. Immunol.* **14**, 337–345 (2013).
96. J. M. Gendron, J.-S. Liu, M. Fan, M.-Y. Bai, S. Wenkel, P. S. Springer, M. K. Barton, Z.-Y. Wang, Brassinosteroids regulate organ boundary formation in the shoot apical meristem of *Arabidopsis*. *Proc. Natl. Acad. Sci. U.S.A.* **109**, 21152–21157 (2012).
97. Y. Li, T. Xia, F. Gao, Y. Li, Control of plant branching by the CUC2/CUC3-DA1-UBP15 regulatory module. *Plant Cell* **32**, 1919–1932 (2020).
98. H. Vanhaeren, N. Gonzalez, F. Coppens, L. De Milde, T. Van Daele, M. Vermeersch, N. B. Eloy, V. Storme, D. Inzé, Combining growth-promoting genes leads to positive epistasis in *Arabidopsis thaliana*. *eLife* **3**, e02252 (2014).
99. T. Murashige, F. Skoog, A revised medium for rapid growth and bio assays with tobacco tissue cultures. *Physiol. Plant.* **15**, 473–497 (1962).
100. M. Karimi, T. B. Jacobs, GoldenGateway: A DNA assembly method for plant biotechnology. *Trends Plant Sci.* **26**, 95–96 (2021).
101. H. Zhang, E. Linster, M. Wirtz, F. L. Theodoulou, Relative protein lifetime measurement in plants using tandem fluorescent protein timers. *Methods Mol. Biol.* **2581**, 201–220 (2023).
102. M. Andriankaja, S. Dhondt, S. De Bodt, H. Vanhaeren, F. Coppens, L. De Milde, P. Mühlenbock, A. Skirycz, N. Gonzalez, G. T. S. Beemster, D. Inzé, Exit from proliferation during leaf development in *Arabidopsis thaliana*: A not-so-gradual process. *Dev. Cell* **22**, 64–78 (2012).
103. J. Van Leene, D. Eeckhout, G. Persiau, E. Van De Slijke, J. Geerinck, G. Van Isterdael, E. Witters, G. De Jaeger, Isolation of transcription factor complexes from *Arabidopsis* cell suspension cultures by tandem affinity purification. *Methods Mol. Biol.* **754**, 195–218 (2011).
104. J. Van Leene, D. Eeckhout, B. Cannoot, N. De Winne, G. Persiau, E. Van De Slijke, L. Vercruysse, M. Dedecker, A. Verkest, K. Vandepoele, L. Martens, E. Witters, K. Gevaert, G. De Jaeger, An improved toolbox to unravel the plant cellular machinery by tandem affinity purification of *Arabidopsis* protein complexes. *Nat. Protoc.* **10**, 169–187 (2015).
105. J. Van Leene, C. Han, A. Gadeyne, D. Eeckhout, C. Matthijs, B. Cannoot, N. De Winne, G. Persiau, E. Van De Slijke, B. Van de Cotte, E. Stes, M. Van Bel, V. Storme, F. Impens, K. Gevaert, K. Vandepoele, I. De Smet, G. De Jaeger, Capturing the phosphorylation and protein interaction landscape of the plant TOR kinase. *Nat. Plants* **5**, 316–327 (2019).
106. J. Van Leene, D. Eeckhout, A. Gadeyne, C. Matthijs, C. Han, N. De Winne, G. Persiau, E. Van De Slijke, F. Persyn, T. Mertens, W. Smagghe, N. Crepin, E. Broucke, D. Van Damme, R. Pleskot, F. Rolland, G. De Jaeger, Mapping of the plant SnRK1 kinase signalling network reveals a key regulatory role for the class II T6P synthase-like proteins. *Nat. Plants* **8**, 1245–1261 (2022).
107. S. Hamperl, C. R. Brown, J. Perez-Fernandez, K. Huber, M. Wittner, V. Babl, U. Stöckl, H. Boeger, H. Tschochner, P. Milkereit, J. Griesenbeck, Purification of specific chromatin domains from single-copy gene loci in *Saccharomyces cerevisiae*. *Methods Mol. Biol.* **1094**, 329–341 (2014).
108. Z. Zhai, H. I. Jung, O. K. Vatamaniuk, Isolation of protoplasts from tissues of 14-day-old seedlings of *Arabidopsis thaliana*. *J. Vis. Exp.*, 1149 (2009).
109. M. W. Pfaffl, A new mathematical model for relative quantification in real-time RT-PCR. *Nucleic Acids Res.* **29**, e45 (2001).
110. J. Vandesompele, K. De Preter, F. Pattyn, B. Poppe, N. Van Roy, A. De Paepe, F. Speleman, Accurate normalization of real-time quantitative RT-PCR data by geometric averaging of multiple internal control genes. *Genome Biol.* **3**, research0034.1 (2002).

Acknowledgments: We would like to thank our colleagues from the VIB Center of Plant Systems Biology, in particular M. Dubois and R. Tenorio Berrio, for all discussions and the nice working atmosphere. We thank D. Inzé for his support and the opportunity to carry out this research in the VIB Center of Plant Systems Biology. We also thank A. Bleys for reading the manuscript. The IP-MS/MS samples were processed by the VIB Proteomics Core (Ghent

University, 9000 Ghent, Belgium). **Funding:** This work was supported by Bijzonder Onderzoeksfonds (BOF08/01M00408 to M.V. and 01SC3117 to Y.C.), China Scholarship Council (201604910566 to Y.C.), Research Foundation Flanders (12V0218N to H.V.), and Research Foundation Flanders (G0E2719N to H.V. and Y.C.). **Author contributions:** Y.C. and H.V. conceived the study. Y.C., M.V., J.V.L., G.D.J., Y.L., and H.V. performed experimentation, data analysis, and data interpretation. Y.C. and H.V. wrote the paper. **Competing interests:** The authors declare that they have no competing interests. **Data and materials availability:** All data needed to evaluate the conclusions in the paper are present in the paper and/or the Supplementary Materials.

Submitted 15 June 2023
Accepted 8 February 2024
Published 13 March 2024
10.1126/sciadv.adj2570